THE UNIVERSITY OF MANITOBA

EXPERIMENTAL INVESTIGATION OF NATURAL CONVECTION FROM A VERTICAL CYLINDER WITH UNIFORM HEAT FLUX AND IN A VERTICAL ANNULUS WITH MIXED BOUNDARY CONDITIONS

By

RAMASWAMI SRINIVASAN

A THESIS SUBMITTED TO THE FACULTY OF GRADUATE STUDIES
IN PARTIAL FULFILLMENT OF THE REQUIREMENTS FOR
THE DEGREE OF MASTER OF SCIENCE OF MECHANICAL ENGINEERING

DEPARTMENT OF MECHANICAL ENGINEERING
WINNIPEG, MANITOBA

AUGUST, 1977

EXPERIMENTAL INVESTIGATION OF NATURAL CONVECTION FROM A VERTICAL CYLINDER WITH UNIFORM HEAT FLUX AND IN A VERTICAL ANNULUS WITH MIXED BOUNDARY CONDITIONS

BY

RAMASWAMI SRINIVASAN

A dissertation submitted to the Faculty of Graduate Studies of the University of Manitoba in partial fulfillment of the requirements of the degree of

MASTER OF SCIENCE

ABSTRACT

An experimental investigation was conducted on the heat transfer across a narrow atmospheric air gap formed by two vertical coaxial cylinders with closed ends. The study, involving laminar free convection, was carried out for the condition of intermixing of the boundary layers. The inner surface was maintained at a constant heat flux, which was varied to change the Grashof number based on gap width, while the outer surface was held isothermal. The gap remained constant as the experiment was carried out with only one heated cylinder-can configuration. The results of the local heat transfer were correlated in the form

$$Nu_x = 0.421\ Gr_x^{*1/5} \quad , \quad 2 \times 10^5 < Gr_x^* < 3 \times 10^{10}$$

A steep rise in overall Nusselt number with Grashof number (based on radial clearance) was noticed. Such a trend is not observed for isothermal cavities and thus suggests the possibility of including surface heat flux as a parameter additional to aspect ratio and radius ratio, in the correlation for overall heat transfer in the asymptotic regime of a vertical annulus. Further experimental data is required to confirm the above dependence. An investigation of unbounded free convection in air using the same heated cylinder was also carried out, and the local heat transfer results correlated by

$$Nu_x = 0.487\ Gr_x^{*1/5} \quad , \quad 5 \times 10^7 < Gr_x^* < 2 \times 10^{10}$$

were in good agreement with other published works.

ACKNOWLEDGEMENTS

The author gratefully acknowledges the guidance and encouragement he received from Dr. A. C. Trupp, over the course of this investigation. The author also wishes to express his thanks to Rita Hanley for typing out the manuscript in its entirety and to the staff and colleagues in the Mechanical Engineering Department for their help and cooperation.

TABLE OF CONTENTS

Page

ABSTRACT i

ACKNOWLEDGEMENTS ii

TABLE OF CONTENTS. iii

LIST OF FIGURES vi

NOMENCLATURE viii

1. INTRODUCTION 1

1.1 Motivation 1

1.2 Objectives and Scope 2

2. LITERATURE REVIEW 4

2.1 Unbounded Free Convection 4

2.2 Natural Convection in Enclosed Spaces 6

3. DESIGN AND THEORETICAL CONSIDERATIONS 13

3.1 Heater Selection 13

3.2 Flow Regimes in Vertical Air Layers 14

3.3 Criteria for Can Selection 15

3.4 Mathematical Formulation 16

4. EXPERIMENTAL SETUP AND PROCEDURE 19

4.1 Heater 19

4.2 Traversing Mechanism 19

4.3 Boundary Layer Measurements in Unbounded Free Convection 19

4.3.1 Velocity Field 19

4.3.2 Temperature Field 21

4.3.3 Test Procedure 21

Page

4.4 Can Design 23

4.5 Test Procedure for Temperature Field in an Enclosed Space 23

5. RESULTS AND DISCUSSION 25

5.1 Unbounded Free Convection 25

5.1.1 General 25

5.1.2 Surface Temperature Variation 26

5.1.3 Boundary Layer Velocity Distribution 27

5.1.4 Boundary Layer Temperature Distribution 28

5.1.5 Local Heat Transfer 28

5.1.6 Heater Surface Emmissivity 31

5.1.7 Overall Heat Transfer 32

5.2 Free Convection in Vertical Annulus 33

5.2.1 Asymptotic Regime 33

5.2.2 Local Heat Transfer 34

5.2.3 Overall Heat Transfer 35

6. CONCLUSION AND RECOMMENDATIONS 39

6.1 Unbounded Free Convection 39

6.2 Natural Convection in Vertical Annulus 39

REFERENCES 42

APPENDIX A: DESIGN AND ANALYSIS OF HEATER 46

1. Design 46

2. Analysis 47

Page

APPENDIX B: CALIBRATION 56

1. Low Velocity Anemometer 56

2. Thermocouples 57

APPENDIX C: SAMPLE CALCULATIONS 58

LIST OF FIGURES

Figure		Page
1	Sketch Showing Different Flow Regimes in Vertical Convection Layers	63
2	Details of Heater	64
3	Traversing Mechanism with Velocity Probe	65
4	Temperature Probe	66
5	Instruments Used for This Investigation	67
6	Details of Can	68
7	Non-dimensional Wall Temperature Distribution	69
8	Local Heat Flux Distribution, Q = 18.11 watts	70
9	Local Heat Flux Distribution, Q = 38.61 watts	71
10	Dimensionless Velocity Distribution for Unbounded Free Convection, Q = 18.11 watts	72
11	Dimensionless Velocity Distribution for Unbounded Free Convection, Q = 38.61 watts	73
12	Dimensionless Temperature Distribution for Unbounded Free Convection, Q = 18.11 watts	74
13	Dimensionless Temperature Distribution for Unbounded Free Convection, Q = 38.61 watts	75
14	Photograph showing Induced Flow near the Leading Edge	76
15	Boundary Layer Temperature Distribution, Q = 18.11 watts.	77
16	Boundary Layer Temperature Distribution, Q = 38.61 watts.	78

Figure		Page
17	Sample Graph to Determine Local Heat Flux	79
18	Local Heat Transfer Results for Unbounded Free Convection	80
19	Temperature Field in Vertical Air Layer, Q = 18.11 watts. .	81
20	Temperature Field in Vertical Air Layer, Q = 29.36 watts. .	82
21	Temperature Field in Vertical Air Layer, Q = 37.76 watts. .	83
22	Local Heat Transfer Results for Vertical Annulus, Using Modified Grashof Number	84
23	Local Heat Transfer Results for Vertical Annulus, Using Conventional Grashof Number	85
24	Overall Heat Transfer Results for Vertical Annulus	86
25	Non-dimensional Heater Wall Temperature Distribution for Vertical Annulus	87
26	Sketch of Calibration Equipment for Low Velocity Anemometer	88
27	Calibration Curves for Low Velocity Anemometer	89

NOMENCLATURE

A	Surface area
C	Specific heat
D	Diameter
g	Gravitational acceleration
H	Height of air layer or gap
h	Convective heat transfer coefficient
K	Thermal conductivity
p	Pressure
Q	Total power input
q	Local heat flux density
R	Radius
r	Distance from cylinder axis
T	Temperature
t	Time
u	Velocity component in r-direction
v	Velocity component in x-direction
W	Width of air gap
x	Axial distance from bottom of cylinder
y	Radial distance from cylinder surface
α	Thermal diffusivity
β	Thermal expansion coefficient
ΔT	Temperature difference
ϵ	Emmissivity

μ	Absolute viscosity
ν	Kinematic viscosity
ρ	Density
σ	Stefan-Boltzmann constant
ψ	Stream function
ω	Vorticity

Subscripts

a	Air
c	Cold wall
H	Based on height
h	Hot wall
m	Maximum
p	At constant pressure
W	Based on gap width
w	Wall
x	Based on axial distance
∞	Ambient
in	inner cylinder
out	outer cylinder

Dimensionless Parameters

Pr	(ν/α)	Prandtl number
Nu	$(\frac{h}{K})$ (distance parameter)	Nusselt number
Gr	$\frac{g\beta}{\nu^2} \Delta T$ (distance parameter)^3	Grashof number
Gr_x^*	$\frac{g\beta}{\nu^2} \frac{q}{K}$ (distance parameter)^4	Modified Grashof number
Ra	(Gr)(Pr)	Rayleigh number

CHAPTER 1

INTRODUCTION

1. Introduction

1.1 Motivation

There are many practical applications involving free convection in enclosed spaces. With the demand for energy in the coming decades to be primarily met by nuclear power, two specific examples involving spent nuclear fuel bundles could be cited. These are the shielded shipping flasks used to transport nuclear fuel bundles after as little as three days decay and the storage tanks used for semi-permanent dry storage after about five years decay. The design of such containers involves an understanding of the free convection process in enclosed spaces.

The process of natural convective flow in enclosed spaces involves two primary surfaces and hence, in addition to their geometry, different boundary conditions are possible. Most of the investigations reported have been for the isothermal rectangular cavity with the side walls maintained at different temperatures. Such a situation is observed in double glazed windows, and many experimental and numerical investigations have been carried out [1, 3, 4, 5].

The convective heat transfer in an enclosed annular cavity formed by concentric vertical cylinders, which simulates a spent nuclear fuel bundle during semi-permanent dry storage in a can, has been given little attention by investigators possibly because it is felt it could be approximated by the rectangular cavity which is a limiting case of the

annulus with a radius ratio of unity. A numerical solution for an annular cavity with isothermal walls was presented by De Vahl Davis and Thomas [6]. The nuclear rod bundle dissipates heat with a uniform surface heat flux thus giving a mixed boundary condition - uniform surface flux plus an isothermal outer wall which is typical of the shipping flask and canned storage applications. Sheriff [2] experimentally investigated the overall heat transfer for such a system using carbon dioxide but this work was done at high Grashof numbers. The present work was undertaken to study the flow at lower Grashof numbers and with air under atmospheric conditions.

1.2 Objectives and Scope

The experimental investigations form the first phase in the study of natural convective heat transfer in enclosed spaces at the University of Manitoba. The present work involved the design of a cylindrical heater capable of low power outputs; the maximum being governed by the teflon core which chars at approximately 550^{o}F and on which the heating element was uniformly wound. The heater was analysed for the surface flux distribution.

The boundary layer velocity and temperature profiles were obtained for the vertical cylinder at different heat flux levels via hot-wire anemometry and a thermocouple probe respectively. The correlations formed for the local and average heat transfer were compared with results available in the literature for unbounded free convection from vertical cylinders and plates. This work was done to establish proficiency in

the use of the measuring devices. In addition, the local heat fluxes arrived at from the temperature profiles were used to estimate the emmissivity of the heater surface. This indirectly determined experimental value was in the range reported in handbooks on physical properties. This value of emmissivity was subsequently used in the second part of the experiment to evaluate the overall heat transfer in a vertical annulus.

The second part of this experimental investigation involved the study of free convective heat transfer in a vertical annulus. The enclosed space was formed by a cylindrical can whose surface was maintained isothermal by circulating cooling water on the outside of the can. The can dimensions were chosen to provide a condition of intermixing of the boundary layers on the two surfaces. Due to time limitations only one can configuration was tested, hence the experimental results reported here must be supplemented in the next phase of the project in order to investigate the effects of aspect ratio and radius ratio on the overall heat transfer.

CHAPTER 2

LITERATURE REVIEW

2.1 Unbounded Free Convection

Natural convection from vertical flat plates and cylinders have been analysed by several investigators with different boundary conditions. Exact solutions of the boundary layer differential equations for the vertical flat plate have been reported by Ostrach [20] for the isothermal case and by Sparrow & Gregg [15] for the uniform surface heat flux. Sparrow and Gregg [15] pointed out that for the vertical flat plate with uniform surface heat flux, the average Nusselt number can be calculated within 5 percent, using the mid-height plate temperature in the correlation for the isothermal vertical flat plate. Results for laminar free convection with a vertical flat plate subjected to a prescribed non-uniform wall temperature or heat flux were reported by Sparrow [35].

Numerical studies with vertical cylinders were made by Sparrow and Gregg [17] who established conditions to evaluate overall heat transfer from circular cylinders using flat plate theory. Their results showed that heat transfer coefficients for cylinders were greater than those for flat plates and were also a function of Prandtl number. Fujii and Uehara [36] presented approximate formulae relating the local Nusselt number for a vertical flat plate and a cylinder for arbitrary temperature or heat flux distribution. Their results, which were independent of the Prandtl number, have been used to compare the present experimental results with those published in the literature.

An analysis of vertical cylinders with uniform surface heat flux was made by Nagendra et al [16]. They classified the cylinders into three categories of long, short, and wires for comparison with those of a flat plate. The cylinder used in the present experimental setup falls under the short cylinder regime as (Ra_D*D/H) is greater than 10^4. The results of Nagendra et al [16] for the cylinder with a uniform surface heat flux operating in the short cylinder region are such that Nusselt numbers are about 5 per cent higher than those for the isothermal flat plate. Sparrow and Gregg [15] had predicted a difference of 10 percent for flat plates under different boundary conditions. The present experimental results for Nusselt number based on diameter are found to agree well with those reported by Nagendra et al [16] for short cylinders.

Experimental investigations of free convection heat transfer from vertical flat plates were carried out by Bartalsky [39] and Hill [40]. Their results for isothermal flat plates were compared to the present results which indicated the heat transfer rates to be higher for the cylinder than those for the flat plate. Experimental investigation of a vertical aluminium plate in air was made by Dotson [41]. Radiation and conduction reduced his plate surface condition to non-uniform heat dissipation. He concluded these effects to be predominant near the leading edge. Gryzagoridis [37] obtained experimental results for laminar free convection in the course of investigating the combined free and forced convection heat transfer from an isothermal vertical plate. He reported good agreement with the accepted power law of $Nu_x = 0.375\ Gr_x^{\frac{1}{4}}$ for Grashof numbers greater than 10^4.

A few investigators studied the effect of the leading edge on the flow characteristics and heat transfer rates. Gryzagoridis [18] obtained experimental results near the leading edge using a Mach-Zender interferometer. His results indicated the Nusselt number to be 20 per cent higher than those evaluated using the classical boundary layer theory. He also mentioned a possible influence of the temperature difference on the Nusselt number for a fixed Grashof number in the region close to the leading edge.

Natural convection flow in the transition and turbulent regions has been investigated and reported in many papers. Godaux and Gebhart [19] made an experimental study to find the point of transition and have included data from various references. These values were used to confirm that the writer's study of unbounded free convection on the vertical cylinder was in the laminar region.

2.2 Natural Convection in Enclosed Spaces

The study of natural convection in enclosed plane air layers was initiated by Mull and Reiher [11] in 1930. Their experimental study was made in air layers enclosed between two isothermal vertical plates. The results were analysed by Jakob [11] in 1946 and expressed in terms of dimensionless parameters. The effect of aspect ratio (H/W) was also observed and included as a parameter in the relation. It was observed that at low Grashof numbers the Nusselt number approached unity and no influence of the aspect ratio was observed. The exponents, 1/4 and 1/3, of the Grashof number demarcated the laminar and turbulent regions. The

results reported pertained only to the overall heat transfer across the air layer.

An interferometric study of the temperature and flow conditions in vertical air layers was carried out by Eckert and Carlson [1] in 1961. Three different regimes, as shown in Fig. 1, were defined based on the temperature profiles. In the conduction regime a linear temperature drop from the hot to the cold plate was observed. Near the floor and ceiling, the profiles were curved near the vertical walls indicating a contribution by convection for these regions. Heat transfer in the central region was mainly by conduction but this did not imply that the air layer was stationary, however the horizontal velocity over this region was zero and hence all the heat was transferred by conduction. At large Grashof numbers and below a certain limit of height to thickness ratio, two separate boundary layers existed along the vertical surfaces of the enclosure while in the central core the temperature was uniform on horizontal planes. The regime between these two extremes, for moderate Grashof numbers, was called the asymptotic regime. The intermixing of the two boundary layers and their subsequent growth together was observed in this regime. The temperature profiles were curved throughout the whole height of the air layer which indicated that convection contributed to the flow of heat from the hot to the cold plate. A small linear drop in the central region showed the contribution of conduction to the overall heat transfer. The limits of these regimes were specified as functions of the aspect ratio and Grashof number based on cavity width.

In the conduction regime the local Nusselt number was unity in the central region. Local and average Nusselt number relations for the starting and departure corners were also presented by Eckert & Carlson [1]. The average Nusselt number was greater than the central region for starting corners while it was less for the departure corners. Local heat transfer results for the other two regimes were similar and were evaluated using the mid-gap temperature. The results for average heat transfer were presented only for the boundary layer regime as a nonlinear relation for the mid-gap temperature was observed for the asymptotic regime. The local heat transfer relations of Eckert and Carlson [1] were used for comparison with the present experimental work.

Experimental results for an isothermal rectangular cavity using fluids with Prandtl number in the range 3 to 30,000 were reported by Emery and Chu [10]. Their results indicated that the Rayleigh number was the pertinent modulus in correlating the Nusselt number. The conduction regime was suggested for Rayleigh numbers below 10^3 in which cases the Nusselt number was unity and independent of aspect ratio. For Rayleigh numbers greater than 10^3, a single expression for Nusselt number was presented showing the dependence of Nusselt number on aspect ratio. This contradicts the findings of Eckert and Carlson [1] who have suggested the applicability of their relation only in the boundary layer regime due to the linear mid-gap temperature gradient.

An interferometric study on vertical air layers was carried out by Dixon and Probert [8]. Their results showed the limits of the various

regimes to be independent of the aspect ratio and hence the Nusselt vs. Grashof number correlation was based only on the gap width.

Results from an experimental study of laminar free convection in a vertical slot having isothermal walls were presented by Elder [9] using medicinal paraffin and silicone oil, with Prandtl number of 10^3, as the fluid medium. Elder [9] also dealt with the visualisation of the primary, secondary and tertiary flows which preceded the onset of turbulence.

Little literature is available on experimental work in free convection, in enclosed spaces, with mixed boundary conditions. Sheriff [2] reported a correlation for overall heat transfer in vertical annuli with mixed boundary conditions. His work was carried out with carbon dioxide under varying pressures. The results indicated an aspect ratio dependence and are valid only in the boundary layer regime. The expression was similar to those of Eckert and Carlson [1] but the heat transfer rates were found to be much higher for the mixed boundary conditions. Macgregor and Emergy [4] reported that this difference could be as high as 30 percent. Their experiments were performed in a rectangular cavity with one wall maintained at a uniform surface flux, and with fluids having Prandtl numbers greater than unity. Their tests were confined to the boundary layer regime. Their correlation based on results for different fluids suggested the Rayleigh number as the pertinent modulus. The unique curve for each fluid, at each value of aspect ratio, indicated a separate Prandtl number dependence (in addition to the aspect ratio) on the overall heat transfer results.

The literature survey on experimental work showed that very little emphasis has been placed on free convection in the asymptotic regime. The present investigation was therefore carried out to obtain a correlation for heat transfer in the asymptotic regime with mixed boundary conditions.

Before reviewing numerical studies, it is appropriate to briefly mention additional work by Elder [42] in regard to laminar-to-turbulent transition. Elder [42] also conducted an experimental investigation of turbulent free convection in a vertical slot. Transition to turbulence was reported around a Rayleigh number of 10^6, and for Rayleigh number above 10^7 the flow in the central part was observed turbulent. The extent of the turbulent region was reported to grow further towards the ends as Rayleigh number was increased. The motion was interpreted in terms of three regimes: the sublayer where the thermal energy transferred by conduction was accumulated, the interior region which was continually stirred, and an intermediate mixing layer.

Numerical studies to explain the phenomenon of laminar free convective heat transfer in enclosed spaces have been carried out by many investigators. Batchelor [3] presented an analytical solution for two dimensional motion in a long rectangular cavity with isothermal vertical walls by solving the continuity, momentum and energy equations. This study was made to determine the thermal insulation of double windows consisting of two glass panes with an air space between them. An empirical relation was suggested for the point of transition to the asymptotic regime. Emergy and Chu [10] assumed the existence of two separate boundary layers

on the vertical surfaces and found their numerical and experimental results to be in agreement only beyond Rayleigh numbers of 3×10^5. They suggested this value to be the limit for the asymptotic regime and for the existence of separate boundary layers on the two surfaces. For laminar flow, the Nusselt number was expressed as a function of Rayleigh number and the aspect ratio.

A finite difference formulation was used by Rubel and Landis [5] to solve the governing equations for the steady two dimensional natural convection, in an enclosed vertical rectangular cavity, with isothermal vertical walls and adiabatic top and bottom walls. Their results, valid only for the boundary layer regime, showed a Prandtl number dependence on the flow configuration but negligible effect on the overall heat transfer relations.

Newell and Schmidt [7] obtained steady state solutions for aspect ratios 1 to 20 and Grashof numbers covering the asymptotic and boundary layer regimes. Their correlations showed the dependence of the Nusselt number on the aspect ratio but the exponent on the Grashof number was found to be higher than those of other investigators.

Macgregor and Emery [4] performed numerical computations to determine the effects of Rayleigh, Prandtl, Grashof numbers and the aspect ratio on the overall heat transfer coefficient. Their results showed that the Rayleigh number was the pertinent modulus in expressing heat transfer relations. The flow regimes were delineated by the appearance of the temperature profiles as shown in Fig. 1. Their numerical computations

were limited to isothermal walls because the viscosity-temperature relationship of fluids had to be considered for the mixed boundary conditions. This required a wide variety of fluids to be treated to obtain a general correlation. They obtained experimental correlations for the mixed boundary conditions, in order to avoid the large computing times needed to work with variable viscosity flow.

Most of the experimental and numerical analyses found in the literature have dealt with plane vertical walls. This is the limiting case of an annular cavity with a radius ratio of unity. De Vahl Davis and Thomas [6] investigated the fluid motion in a closed annular cavity, with isothermal walls, using a numerical technique. They pointed the dependence of the Nusselt number on the radius ratio in addition to the aspect ratio but no general correlation involving the radius ratio was presented by them.

CHAPTER 3

DESIGN AND THEORETICAL CONSIDERATIONS

3.1 Heater Selection

The heater was designed to simulate a single irradiated CANDU fuel bundle after a five year decay period. The total heating effect of this fuel bundle was ascertained [34] as 10 to 15 watts. The heater was thereby made to the following specifications:

outside diameter = 3.25"

overall length = 20.50"

operating power = 15 watts

The maximum power was restricted to the heating element temperature of 550^{o}F at which the teflon on which the element is wound begins to char.

The test surface made of stainless steel AISI 316 was ground to the following dimensions:

outside diameter = 3.25" ± 0.002"

Taper = 0.0015"/ft.

Surface finish = 63 μ.

The cross-sectional details and analysis of the heater are dealt with in Fig. 2 and Appendix A respectively. The experimental data for heater surface heat flux distribution is shown in Figs. 8 and 9. Also plotted are the predicted local heat fluxes from a finite difference technique used to obtain the surface temperature distribution. These show the variation to be within 10 percent in the central two-thirds

region while at the ends the deviation from the mean is about 20 percent. The end losses are due to convection and radiation from the end surfaces.

3.2 Flow Regimes in Vertical Convection Layers

Fig. 1 shows the various flow regimes for free convective flow in enclosed vertical air layers at atmospheric pressure. Typical temperature profiles are also inserted for the various regimes.

In the conduction regime heat is transferred purely by conduction in the central part of the air layer. The horizontal velocity in the central region is zero and hence no heat transport is connected with the flow. The temperature gradients are linear in this region while they are distorted near the ends where convection contributes to the transfer of energy.

A modest circulatory flow characterises the asymptotic regime. The temperature profiles are curved throughout the height of the air layer implying that convection contributes to the heat flow from the hot to the cold wall. The boundary layers on the hot and cold walls grow in opposite directions and merge with one another but gaseous conduction remains a dominant heat transfer mechanism.

Finally in the boundary layer of the laminar flow regime, heat is transferred primarily by convection in the boundary layers and minimally by conduction through the central core.

The limits of the different regimes are not sharply defined and various relationships have been proposed to delineate them.

Batchelor [3] theoretically derived the limits of the conduction regimes as

$$Gr_W = 695\ (H/W)$$

Eckert and Carlson [1], from their interferometric study, found the limits of these regimes were functions of both the Grashof number and the aspect ratio. Macgregor and Emery [4] and Elder [9] suggested the use of Rayleigh number as the criterion for the various flow regimes. Jakob [11] suggested $Gr_W \simeq 2000$ for transition from conduction to asymptotic flow while Elder [9] experimentally obtained the limit as $Ra_W > 1770\ (H/W)$.

The experimental results of Dixon and Probert [8] indicated the limits of the various regimes are independent of the height and a function of only the Grashof number based on cavity width. This contradicts the findings of other investigators and their limit of the asymptotic regime is much lower than that suggested by others.

3.3 Criteria for Can Selection

In the first phase of study within enclosed spaces it was decided to work in the asymptotic regime. The widely varying limits of the various regimes presented above complicated the selection of can dimensions. Nevertheless the asymptotic flow was assumed to exist within the following limits:

$$3 \times 10^3 < Ra_W < 4 \times 10^4$$

With 20W power input (typical):

Average heater surface temperature = $125^{o}F$

outer can temperature = $75^{o}F$

Mean temperature for fluid properties = $100^{o}F$

ρ_a = 0.0710 lbm/ft^3

μ = 0.0460 lbm/hr.ft.

β = 1/T = 1.79×10^{-3} $1/^{o}F$

For air Pr = 0.72

$Ra_W = (6.39 \times 10^7)W^3$

Hence W = 1.08" , for $Ra_W = 4 \times 10^4$

The can was made from round seamless carbon steel tubing procured from M/S Lyman Tube and Supply Limited. The tubes were available in steps of 1/4" on the inside diameter. A 4-3/4" I.D. tubing was chosen to provide a radial clearance of 3/4" over the heater.

For the can chosen and with 20 watt power input to the heater, $Ra_W = 1.56 \times 10^4$ which is well within the asymptotic region.

The dimensions of the can were:

Inside diameter = $4.75" \begin{smallmatrix} - 0.014" \\ + 0.000" \end{smallmatrix}$

Wall thickness = 1/4"

Overall length = 20.50"

Radial clearance = $0.75" \begin{smallmatrix} - 0.008" \\ + 0.001" \end{smallmatrix}$

3.4 Mathematical Formulation

Numerical studies in steady state two dimensional natural convection in enclosed spaces have been carried out by various investigators

[Ref. 4 to 7]. These dealtmainly with vertical isothermal walls with horizontal insulated or adiabatic surfaces.

This section presents the governing differential equations to be solved along with the necessary boundary conditions in order to obtain a numerical solution for heat transfer in a vertical annulus subjected to mixed boundary conditions.

The time dependent governing equations are as follows:

Mass balance:

$$\frac{\partial \rho}{\partial t} + \frac{1}{r} \frac{\partial}{\partial r} (\rho r u) + \frac{\partial}{\partial x} (\rho v) = 0 \tag{1}$$

Momentum balance:

In the radial direction:

$$\rho\left[\frac{\partial u}{\partial t} + u \frac{\partial u}{\partial r} + v \frac{\partial u}{\partial x}\right] = - \frac{\partial p}{\partial r} + 2 \frac{\partial}{\partial r} \left(\mu \frac{\partial u}{\partial r}\right) + \frac{\partial}{\partial x} \left[\mu\left(\frac{\partial u}{\partial x} + \frac{\partial v}{\partial r}\right)\right] + 2 \frac{\mu}{r} \left[\frac{\partial u}{\partial r} - \frac{u}{r}\right] \tag{2}$$

In the axial direction:

$$\rho\left[\frac{\partial v}{\partial t} + v \frac{\partial v}{\partial r} + u \frac{\partial v}{\partial x}\right] = \rho g \beta \, (T - T_o) - \frac{\partial p}{\partial x} + 2 \frac{\partial}{\partial x} \left(\mu \frac{\partial v}{\partial x}\right) + \frac{1}{r} \frac{\partial}{\partial r} \left[\mu r \left(\frac{\partial u}{\partial x} + \frac{\partial v}{\partial r}\right)\right] \tag{3}$$

Energy balance:

$$C_p \left(\frac{\partial T}{\partial t} + u \frac{\partial T}{\partial r} + v \frac{\partial T}{\partial x}\right) = \frac{1}{r} \frac{\partial}{\partial r} \left(r K \frac{\partial T}{\partial r}\right) + \frac{\partial}{\partial x} \left(K \frac{\partial T}{\partial x}\right) \tag{4}$$

The viscous dissipation term is neglected and the Boussinesq approximation for the buoyancy term, is used.

The above equations are usually recast in terms of the stream function and vorticity which are defined as follows:

Stream function ψ:

$$u = \frac{1}{r}\frac{\partial \psi}{\partial x} \qquad \text{and} \qquad v = -\frac{1}{r}\frac{\partial \psi}{\partial r}$$

Vorticity ω:

$$\omega = \left(\frac{\partial u}{\partial x} - \frac{\partial v}{\partial r}\right)$$

The stream function, vorticity and energy equations are solved subject to the following boundary conditions:

$r = R_{in}$ for all x,

$$u = v = 0$$

$$k\frac{\partial T}{\partial r} = -q_w$$

$r = R_{out}$ for all x,

$$u = v = 0$$

$$T = \text{const.}$$

$x = 0$ for all r,

$$u = v = 0$$

$$\frac{\partial T}{\partial x} = 0$$

$x = H$ for all r,

$$u = v = 0$$

$$\frac{\partial T}{\partial x} = 0.$$

The governing equations are typically solved by expressing them in a finite difference form.

CHAPTER 4

EXPERIMENTAL SETUP AND PROCEDURE

4.1 Heater

The test surface for the cylindrical heater, 3-1/4" diameter and 20-1/2" long, was made of stainless steel AISI 316. The instrumentation of this heater consisted primarily of 30 iron-constantan thermocouples located as indicated in Fig. 2. The constructional details and an analysis of the heater are given in Appendix A.

4.2 Traversing Mechanism

Fig. 3 shows the traversing mechanism clamped on to a camera tripod. This mechanism was used for exact positioning of both the velocity and temperature measuring probes. Radial movements of the probe were obtained through the DISA 55 H01 traversing mechanism. This was mounted on two vernier calipers which provided movements in the horizontal plane and was used to locate the radial direction. Adjustments in the vertical plane was achieved through the camera tripod.

4.3 Boundary Layer Measurements in Unbounded Free Convection

4.3.1 Velocity Field

Various methods have been proposed for the measurement of the velocity field. The optical method uses a photographic technique to measure the trajectories of dust particles carried with the flow while the conventional hot wire anemometer works either as a constant current

or constant temperature anemometer. The basic problem in using the latter at low velocities is the interaction between free and forced convection. As shown in Ref. [29] there is a marked difference in the output for the extreme cases of free convection aiding and opposing forced convection.

In the present investigation the boundary layer velocity was measured with a DISA Type 55 D 80/81 low velocity anemometer. The transducers of this anemometer contain a vibrating probe holder consisting of a printed circuit board with two coils moving in magnetic fields created by two permanent magnets fixed to the housing. One coil acts as the drive coil while the other is the velocity pickup. An oscillator drives the probe holder at a frequency of approximately 250 Hz and an amplitude of ± 0.03 mm. In the low velocity mode the anemometer is used in the range 0 - 30 cms/sec. In the higher range up to 2 m/sec the unit functions as a conventional constant current anemometer. The calibration of this low velocity anemometer is explained in Appendix B.

In measuring the velocity field the transducer of the low velocity anemometer was rigidly clamped to the guide tubing (DISA 55 H 140) of the traversing mechanism. The radial position for the transducer or probe axis with respect to the heater rod was achieved by initially bringing the transducer/probe axis to a position tangent to the heater rod. The probe was retracted and then the DISA traversing mechanism was moved horizontally on the vernier calipers through half the heater rod diameter. With this procedure the maximum offset with respect to the true radial direction was 0.015". By closing an external electrical circuit the probe was brought into contact with the heater surface. The probe was

then moved outwards using the DISA 55 H 01 traversing mechanism and hence the only error introduced in the radial positioning was due to the traversing mechanism which has a resolution of 0.1 mm. The probe position in the vertical direction was measured to within 1/32".

4.3.2 Temperature Field

The temperature distribution in the boundary layer was measured using an iron-constantan thermocouple probe. As shown in Fig. 4, a small portion of the thermocouple wire preceding the hot junction was placed parallel to the test surface. This was done in order to reduce the conduction loss. A similar method was adopted by Vliet and Liu [38] to reduce the conduction losses.

The thermocouple wires were supported in a 0.07" diameter hypodermic needle which was rigidly clamped to the guide tube of the DISA traversing mechanism. The same procedure as mentioned above in the velocity field measurement was adopted to set the probe in a radial direction. The thermocouple calibration procedure is outlined in Appendix B.

4.3.3 Test Procedure

The entire test was carried out in an environmental room (nominal size 7' x 10' x 8'5" high) manufactured by Coldstream Products of Canada Limited, and located in Room 329, Engineering Building. The environmental room was equipped with twelve 2" diameter instrument ports with screw closures on the inside and outside. The heater was allowed to rest freely on a teflon boss 1-1/2" diameter and 1" high. This was enough to clear

the thermocouple wires coming out of the bottom face of the heater. The power supply leads, thermocouple extension wires and the cable from the low velocity anemometer were brought out of the room through one of the instrument ports. This port was also plugged with stuffing from both sides of the wall to avoid any disturbance in the flow field due to stray currents. The room temperature variation during the period required for a complete test was within $\pm$ 0.75^{o}F.

A regulated d.c. power supply system, Model LA 80-3M, from Technipo Inc., was used as the source for the heater; the power input being read from a digital multimeter. A 28-position selector switch was used for the thermocouples, all of which were referenced to an ice bath and read on a Keithley multimeter Model 165. The output from the low velocity anemometer was read through a DISA digital voltmeter Type 55D31. Fig. 5 shows the instrumentation for study of unbounded free convection from the vertical cylinder.

Steady state conditions were achieved 12-14 hours after the power to the heater was switched on. Surface temperatures, read by the built-in thermocouples were recorded both before and after the test. Samples of the thermocouple wire from the same spool as used for the built-in T/C were also calibrated. Ambient temperature during the course of an entire test was 78^{o} $\pm$ 1^{o}F.

Boundary layer measurements were made by moving the probe radially outwards from the heater surface, which was taken as the reference. This reference surface was located by moving the probe into contact with the heater surface and thereby closing an external electrical circuit. Steady

state flow between any two readings was achieved in 20-30 minutes. Barometric pressure and the relative humidity were recorded to make correction on the air density.

4.4 Can Design

Fig. 6 shows the constructional details of the can made from a 4-3/4" inside diameter carbon steel seamless tubing. The tubing was provided with a sheet metal cooling water jacket to maintain the surface isothermal. Cylindrical pins, long enough to project outside the water jacket, were brazed to the seamless tubing and the water jacket. Radial guide holes were drilled through these pins and plugged, when not in use, by collared pins. The hypodermic needle, supporting the thermocouple probe, was guided by a collared bush having a running fit in the guide holes. The collared pin and the bush remained flush with the inside surface of the tubing.

Acrylic end caps centralised the can with the heater giving a radial clearance of $3/4" \begin{smallmatrix} + 0.005" \\ - 0.020" \end{smallmatrix}$. The caps also helped reduce end losses by conduction. The bottom cap with three resting pins supported the entire can assembly.

4.5 Test Procedure for Temperature in Enclosed Spaces

The input to the heater was from the regulated d.c. power supply system mentioned in Section 4.3.3. Steady state conditions were achieved after 12 hours which was indicated by stationarity of the surface temperatures recorded by the built-in thermocouples. A rise of 0.5 F^{o} between

the inlet and outlet cooling water temperatures was permitted. The nominal cooling water temperature during the course of an entire test was $66^{o} \pm 1^{o}F$. The can inner surface was considered isothermal with a surface temperature variation of less than $0.5^{o}F$ during any one test run.

The temperature field in the enclosed space was probed with an iron-constantan thermocouple. The hypodermic needle supporting the thermocouple was guided in the radial direction by the collared bush in the can. The probe was moved radially outwards from the heater surface which was taken as the reference. The procedure for locating the reference surface is outlined in Section 4.3.3. The radial movement of the probe was obtained from the traversing mechanism described in Section 4.2.

CHAPTER 5

RESULTS AND DISCUSSION

The results of the unbounded free convection and natural convection in a vertical annulus are presented separately in the following subsections.

5.1 Unbounded Free Convection

5.1.1 General

Tests were conducted for two different power inputs to the heater, viz., about 18 watts and 39 watts. The modified Grashof number at the top end of the cylinder, for the larger power input, was 1.5×10^{10}. According to the transitional data compiled from various references and presented by Godaux and Gebhart [19] the flow is laminar for $Gr_x^* < 1.4 \times 10^{11}$. The flow for both the power inputs was therefore expected to be laminar and this was confirmed by the anemometer outputs which showed neglibible velocity fluctuations.

Most of the heat transfer results reported in the literature have been for isothermal vertical flat plates. Sparrow and Gregg [17] have established criteria to use flat plate theory for a cylinder giving a maximum error of 5 percent in overall heat transfer results. Fujii and Uehara [36] have presented approximate formulae for calculating the local convective heat transfer coefficient for a cylinder in terms of the corresponding values for a flat plate under similar boundary conditions. Nagendra et al [16] have classified cylinders under three categories of

long, short and wires. For a short cylinder the correlations showed a maximum deviation of 5 percent in overall heat transfer results, if the results for the constant heat flux cylinder are evaluated using an isothermal surface approximation with mean wall temperature. Thus a maximum difference of about 10 percent in overall heat transfer results was envisaged in comparing the results of the present investigation with those of flat plates.

5.1.2 Surface Temperature Variations

Fig. 7 shows the non-dimensional temperature distribution along the cylinder surface. The wall temperatures are those measured by the built-in thermocouples. Also shown is the exact solution of Sparrow and Gregg [15] for a flat plate. The trend for both non-dimensional temperature profiles is almost identical. The deviation from the exact solution is maximum at the lower end due to end convection. End losses/axial conduction cause the reversal in the temperature profile near the top end. (Refer to Appendix C for end loss calculations.)

Figs. 8 and 9 show the variation of local heat flux along the cylinder surface. Also plotted are the average surface heat fluxes (obtained from the power input to the heater less the radiation losses from the heater surface) and the surface heat flux distribution obtained analytically using heat transfer correlations for a vertical flat plate (see Appendix A). From these Figures, the surface heat flux distribution is seen to be fairly uniform in the central region where the maximum deviation from the average value is about 10 percent for both the power

inputs. In addition to end convection effects, the non-uniform heat flux distribution is also due to axial heat conduction within the heater (see Appendix A).

5.1.3 Boundary Layer Velocity Distribution

The velocity field was measured with a DISA low velocity anemometer. No significant velocity fluctuations were observed during these measurements which indicated laminar flow and the absence of any significant stray currents in the room. The boundary layer thickness was about 3/4" at the top for the higher heat flux and the maximum velocity recorded by the anemometer was about 29 cm/sec.

The non-dimensional velocity distributions are shown in Figs. 10 and 11 for the two different power inputs. The fluid properties were evaluated at the mean of the average wall temperature and the ambient. Atmospheric corrections were made for the air density. The experimental points are scattered around the exact solution of Ostrach [20] which is based on boundary layer assumptions. Exact agreement was not expected due to the different geometry and boundary conditions. The experimental points show that the boundary layer assumption is not valid near the leading edge since the flow starts ahead of the leading edge. The leading edge effect is seen in Fig. 14. The results of Ostrach indicate a Prandtl number dependence of these dimensionless plots. The value adopted in these plots was 0.72; using slightly higher values would shift the curve towards the experimental points.

5.1.4 Boundary Layer Temperature Field

The temperature field was mapped with the iron-constantan thermocouples calibrated as explained in Appendix B. The non-dimensional plots are shown in Figs. 12 and 13. The exact solution of Ostrach [20] for an isothermal vertical plate is also shown in the Figures. Due to the different geometry and surface conditions exact agreement was not expected. However, the closer agreement of the experimental data for the higher heat flux in Fig. 13 suggests that the surface behaves more as an isothermal surface with is attributed to end convection losses and axial conduction within the cylinder. The solution of Ostrach [20] is based on boundary layer assumptions which as already mentioned is not valid close to the leading edge. For the case of the higher heat flux, the boundary layer grows much faster and so the boundary layer assumptions are applicable much closer to the leading edge as compared to the lower heat flux. This partly explains the better agreement of data in Fig. 13, as compared to Fig. 12, near the leading edge. The scatter of points closer to the boundary layer edge is possibly due to slight air turbulence within the experimental chamber.

5.1.5 Local Heat Transfer

Figs. 15 and 16 show the smoothed temperature distributions in the boundary layer. The temperature scales belong to two of the profiles while the rest are arbitrarily shifted in the vertical direction.

Sample calculations for evaluating the local heat transfer coefficient are shown in Appendix C. Fig. 17 illustrates the graphical

determination of the local heat flux. The error due to graphical determination of the slope was within 10 percent of that obtained analytically using a forward difference technique. Since equal displacement steps were not used while probing the temperature field close to the wall, the graphical technique for slope determination was adopted in lieu of employing interpolated values for a numerical evaluation. The local flux distributions are plotted in Figs. 8 and 9. The experimental points for the local Nusselt and modified Grashof numbers are shown in Fig. 18. The eight data points away from the leading edge were correlated using least-square-fit by:

$$Nu_x = 0.487\ Gr_x^{*1/5}$$

with a standard deviation (σ) of 1.5×10^{-3}.

For comparison with the results from other references the modified Grashof number is expressed as a product of the conventional Grashof and Nusselt number as shown below:

$$Gr_x^* = \left(\frac{g\beta}{\nu^2}\right)\left(\frac{q}{K}\right) x^4$$

$$= \left(\frac{g\beta}{\nu^2}\right)\left(\frac{x^4}{K}\right) h_x\ (T_w - T_\infty)$$

$$= \left[\left(\frac{g\beta}{\nu^2}\right)(\Delta T)(x^3)\right]\left(\frac{h_x \cdot x}{K}\right) = Gr_x \cdot Nu_x$$

Hence the correlation may be rewritten as:

$$Nu_x = 0.407\ Gr_x^{1/4}$$

Summarised below are the results from other references:

For isothermal vertical flat plate:

Ostrach [20]	$Nu_x = 0.356\ Gr_x^{1/4}$
Hill [40]	$Nu_x = 0.360\ Gr_x^{1/4}$
Churchill and Ozoe [21]	$Nu_x = 0.357\ Gr_x^{1/4}$
Gryzagoridis [37]	$Nu_x = 0.375\ Gr_x^{1/4}$

For uniform surface heat flux,

Vertical flat plate:

Sparrow and Gregg [15]	$Nu_x = 0.417\ Gr_x^{1/4}$
Churchill and Ozoe [21]	$Nu_x = 0.404\ Gr_x^{1/4}$

The present experimental results are in good agreement with that of Sparrow and Gregg [15] and Churchill and Ozoe [21] for a flat plate. However for a cylinder the results were expected to be higher, but this may be due to the fact that the surface flux was not completely uniform over the length of the cylinder. Using the formula of Fujii and Uehara [36] for uniform heat flux to convert the results of Churchill and Ozoe [21] for flat plate to cylinder, the present results were about 10 percent low at the leading edge and less than 5 percent low in the central region. Correspondingly, using the formula of Fujii and Uehara [36] for isothermal surface and the results of Ostrach [20], the present results were around 5 percent high at the leading edge and this increased along the length of the cylinder. These results indicate the heat transfer rates to be greater for a cylinder with uniform heat flux as compared to those for a flat plate.

5.1.6 Heater Surface Emmissivity

A direct measuring device for the emmissivity of the stainless steel heater surface was not available. Hence emmissivity was evaluated (for later use) by indirect measurement. Heat loss by radiation from the cylinder surface was calculated based on an allowance for free convective and radiative heat loss from the top face and by employing the experimentally determined average surface heat flux. Appendix B shows the calculations for emmissivity. Values of 0.291 and 0.295 were obtained for the two power inputs considered.

Reference books on thermophysical properties were consulted to obtain typical published value. The table below gives the emmissivity from these references:

Stainless steel AISI 316:

Reference		Surface Condition	ε
Touloukian	[22]	As received and wiped	0.3
Wood and others	[23]	Cleaned	.28/.32
Touloukian	[24]	Cleaned	.23/.39
Goldsmith	[25]	Cleaned	.28/.31
Hottel	[26]	Soap water cleaned	.28
Siegel	[27]	Polished	.23

The probable emmissivity was therefore in the range of 0.23 to 0.39. A value in the lower half of this range (0.23 - 0.31) was anticipated since

the formation of any significant iron oxide on the surface was considered remote due to the low operating temperatures, whereas a fine layer of chromium oxide was expected. The value of 0.29, being in good agreement, was therefore adopted. The reliability of this value was to some extent confirmed since by using it to predict the heater surface temperature analytically a maximum deviation of 4 percent was obtained.

5.1.7 Overall Heat Transfer

The overall heat transfer was calculated on the basis of both the height and the diameter. Based on height, the result was:

$$Nu_H = A\,(Ra_H)^{1/4}$$

where $A = 0.576 \pm 2\%$ for the two determinations. Ostrach [20] obtained a value of 0.411 for the isothermal plate. Such a low value was mainly due to the boundary layer assumptions. The present results are 5 percent higher than that of Gryzagoridis [18] who considered the leading edge effects on an isothermal vertical flat plate. The empirical relations of references [12] and [13] are 8 to 10 percent lower than the present results. This is due to the different geometry and boundary condition employed in the present investigation.

Based on diameter, the result was:

$$Nu_D = A\,(Ra_D \frac{D}{H})^{1/4}$$

where $A = 0.576 \pm 2\%$.

This is about 4 percent lower than that suggested by Nagendra et al [16], who numerically obtained a value of $A = 0.6$ for short cylinders with

uniform surface heat flux. Due to the limited data a general conclusion cannot be drawn but the agreement for the two data points considered is good.

5.2 Free Convection in Vertical Annulus

5.2.1 Asymptotic Regime

The temperature field in the air filled cavity was investigated for three different power inputs to the central heater while the outside surface temperature was held constant at a nominal value of $66^{o}F$ by circulating cooling water through the outer jacket. Grashof numbers based on cavity width (Gr_{W}) and evaluated using the average heated surface temperature were in the range 2.0 to 3.4 x 10^{4}. From various references [1, 4, 8, 9] , the flow in the annulus, for the above Grashof numbers, is considered in the asymptotic regime. This fact is also confirmed from the temperature profiles shown in Figs. 19 to 21. The profiles are non-linear over the entire height of the cavity except for a small linear portion in the central region. In this region of the cavity, the horizontal velocity is zero and heat transfer is purely by conduction while in the regions towards the corner, convection contributes to the overall heat transfer from the hot to the cold surface. The boundary layers, developing in opposite directions on the two surfaces, have met and grown together. Hence a numerical analysis for this regime based on the existence of separate boundary layers in incorrect.

5.2.2 Local Heat Transfer

Figs 22 and 23 show the graph of local Nusselt vs. Grashof numbers for the asymptotic regime. Fluid properties were evaluated at the mean of average hot wall and cold wall temperatures. Sample calculations are shown in Appendix C. Using least square fit the experimental points were correlated as

$$Nu_x = 0.421\ Gr_x^{*1/5}$$

with a standard deviation (σ) of 7.2×10^{-2}. The correlation expressed in terms of the conventional Grashof number is

$$Nu_x = 0.339\ Gr_x^{1/4}.$$

Fig. 23 shows the plot of Nu_x vs. Gr_x. Also shown on the same graph is the correlation of Eckert and Carlson [1] for an isothermal rectangular cavity. The non-dimensional Grashof and Nusselt numbers in Eckert and Carlson's correlation were based on temperature difference using the local mid gap temperatures. Thus a direct comparison of the correlations is misleading. Assuming the mid gap temperature to be the average of the hot and cold wall temperatures (this is a good approximation for locations away from the ends of the cylinder) Eckert and Carlson's [1] correlation can be expressed as

$$Nu_x = 0.094\ Gr_x^{0.3}$$

where the Nusselt and Grashof numbers are now based on the temperature difference between the hot and cold wall temperatures. The experimental

results for the mixed boundary conditions are now seen to be much higher than those given by the above correlation of Eckert and Carlson [1] for isothermal surfaces. This confirms the findings of Macgregor and Emery [4].

5.2.3 Overall Heat Transfer

In any convective heat transfer process the parameter of greatest importance is the overall Nusselt number. Fig. 24 shows the plot of Nu_w vs. Gr_w from various references along with the experimental points for the three different power inputs considered. The overall Nusselt and Grashof numbers were evaluated using the temperature difference between the walls of the annulus, the hot wall temperature being obtained by averaging over the entire length of the heater. The surface heat flux used in defining the Nusselt number was obtained from the power input to the heater less heat lost by radiation from all the surfaces and convection loss from the top and bottom surfaces of the heater. From Fig. 24 the following observations can be made:

(i) Radius ratio and aspect ratio:

The annular ratio investigated was 1.46. Comparison of the present experimentally obtained Nusselt numbers is made with the results of Newell and Schmidt [7], Jakob [11] and McAdams [12] which are valid for flow in isothermal rectangular enclosures - a limiting case of an annulus with a radius ratio of unity. Their results expressed in the form $Nu_w = A\ (Gr_w)^B\ (H/L)^C$ are about 30 percent lower than the experimental values. One could thus cautiously accept this increase in Nusselt

number as being due to the increased radius ratio. Physically this increase in heat transfer rate is due to greater disturbance of the isotherms in the end regions of the cavity. The above observations are in agreement with the numerical results of De Vahl Davis and Thomas [6] shown in Fig. 24.

The effect of changing aspect ratio was not studied in the present investigation. The heat transfer rates are expected to decrease with increase in aspect ratio due to increased boundary layer interference and the proportional increase in the importance of conductive heat transfer in the central region.

(ii) Boundary conditions:

The results of the present investigation are 40 to 80 percent higher than those of Emery and Chu [10] for isothermal rectangular cavities. This difference is due to the combined effects of geometry and the boundary conditions of the system. As discussed in (i) the effect of radius ratio is to increase the heat transfer rates by about 30 per cent and from the results of DeVahl Davis and Thomas [6] shown in Fig. 24 the Nusselt number increases by 40 percent with the doubling of the radius ratio. Thus an increase of up to 40 percent in heat transfer rate may be due to the different boundary conditions. This is in agreement with the findings of Macgregor and Emery [4] whose results for the mixed boundary condition are 30 percent higher than that for the isothermal case. Similar conclusions are seen in the boundary layer regime by comparing the results of Sheriff [2] and Eckert and Carlson [1].

(iii) Heat flux level:

The overall Nusselt number was evaluated after making corrections for radiation losses from the heater surface. As explained in Sec. 5.1.6, an emmissivity of 0.29 for the heater surface was used. A line faired through the three data points of Fig. 24 for the average Nusselt number is seen to have a much steeper slope than those of previous correlations. This suggests (superficially) that Nu_w may additionally be dependent on heat flux level in the asymptotic region. This outcome is somewhat surprising, and must be treated with caution; more data is needed to establish or refute this point. The data has been carefully checked and the accuracy is estimated to be within 20%. A variable systematic error could account for the discrepancy but no basis for such an error could be uncovered. The assumed value for the emmissivity of the outer surface ($\varepsilon_2 = 0.8$) may be high, but reducing ε_2 only accentuates the apparent heat flux dependence. Heat transfer by radiation was also re-assessed using local hot surface temperatures (averaged over short vertical intervals) but the total heat transfer by radiation did not change appreciably compared to using the overall average hot wall temperature. It is possible that the phenomenon is a characteristic of the experimental apparatus which is related to departure from the uniform heat flux. A completely uniform heat flux distribution for the hot surface would result in a distribution of surface temperature which increases monotonically with height. As shown in Fig. 25, the actual surface temperature peaks before the top. This leads to lower average

hot surface temperatures than the ideal case. This lower temperature difference (difference of average hot wall temperature and the cold wall temperature), which is used to compute Nu_w, may possibly have resulted in abnormally high Nusselt numbers. In any event, as already mentioned, more experimental work is required to adjudicate the point. In the meantime, the possibility would appear to exist that in the asymptotic region, Nu_w is dependent on the heat flux level in addition to the Rayleigh number, aspect ratio and the radius ratio.

CHAPTER 6

CONCLUSIONS AND RECOMMENDATIONS

The following conclusions can be drawn from the experimental results presented in the previous chapters:

6.1 Unbounded Free Convection

The local natural convective heat transfer results for a vertical cylindrical surface maintained at a constant heat flux can be expressed as

$$Nu_x = 0.487\ Gr_x^{*1/5}, \quad 5 \times 10^7 < Gr_x^* < 2 \times 10^{10}$$

Agreements with the theoretical predictions of Sparrow and Gregg [15] and Churchill and Ozoe [21] for vertical plane walls with uniform flux density are good. The deviation of the experimental points at low Grashof numbers is very likely due to the induced flow near the leading edge. The effect of the leading edge is clearly evident by comparing the present average Nusselt numbers with the numerical evaluation of Ostrach [20]. There is good agreement with Gryzagoridis' [18] correlation for an isothermal flat plate considering the leading edge effect. The higher values from the present investigation are due to the different boundary conditions and the geometry of the system.

6.2 Natural Convection in Vertical Annulus

(i) The temperature profiles of Figs. 19 to 21 are curved over the entire height except for a small linear drop in the central region.

This shows that in the asymptotic region both conduction and convection contribute to the transfer of heat from the hot to the cold surface.

(ii) The local heat transfer results are correlated as

$$Nu_x = 0.421\ Gr_x^{*1/5} \quad , \qquad 2 \times 10^5 < Gr_x^* < 3 \times 10^{10}$$

The results are in good agreement with those of Eckert and Carlson [1]; the difference occurring due to the geometry and the boundary conditions.

(iii) The average Nusselt numbers are approximately 30% higher than those for a vertical plane cavity indicating that the radius ratio must be included as a parameter in expressing the overall heat transfer relation.

(iv) The boundary conditions have a profound effect on the heat transfer rates. Comparison with previously published results for an isothermal plane cavity indicate that the Nusselt numbers are up to 40% higher for the mixed boundary layer system. This is in agreement with the results of Macgregor and Emery [4].

(v) The steep slope of a line faired through the three experimental points suggests that in the asymptotic region Nu_w may also be dependent on the heat flux level. Additional data is required to settle this point.

It is concluded that the overall heat transfer in vertical cylindrical annuli is a complex function of many parameters in the asymptotic regime. Most of the work reported in literature has been on plane rectangular cavity with isothermal walls. In the present experimental investigation, it was observed that the overall Nusselt number depends on the boundary conditions, Grashof number, radius ratio, aspect

ratio and possibly the heat flux level. Thus future research must be directed towards investigating the exact nature of the effect of these parameters. For the existing heater, the inner boundary condition is fixed. It is therefore suggested that cans of different diameters be used to alter the radius and aspect ratios, in the asymptotic regime for which few experimental results are available. This may enable a single correlation to be formulated in expressing the overall heat transfer within enclosed spaces. Such a correlation would have immense practical use.

REFERENCES

1. Eckert, E. R. G. and Carlson, W. O., "Natural Convection in an Air Layer Enclosed between Two Vertical Plates with Different Temperatures", Int. J. Heat Mass Transfer, V. 2, 1961, pp. 106-120.

2. Sheriff, N., "Experimental Investigation of Natural Convection in Single and Multiple Vertical Annuli with High Pressure Carbon Dioxide". Proceedings of the Third International Heat Transfer Conference, Vol. II, 1966, pp. 132-138.

3. Batchelor, G. K., "Heat Transfer by Free Convection Across a Closed Cavity Between Vertical Boundaries at Different Temperatures". Quarterly of Applied Mathematics. Vol. 12, 1954, pp. 209-233.

4. Macgregor, R. K. and Emery, A. F., "Free Convection through Vertical Plane Layers - Moderate and High Prandtl Number Fluids". Journal of Heat Transfer, ASME, Series C. Vol. 91, 1969, pp. 391-403.

5. Rubel, A. and Landis, F., "Numerical Study of Natural Convection in a Vertical Rectangular Enclosure". The Physics of Fluids, Supplement II, 1969, pp. 208-213.

6. De Vahl Davis, G. and Thomas, R. W., "Natural Convection between Concentric Vertical Cylinders". The Physics of Fluids, Supplement II, 1969, pp. 198-204.

7. Newell, M. E. and Schmidt, F. W., "Heat Transfer by Laminar Natural Convection within Rectangular Enclosures". Journal of Heat Transfer, ASME, Vol. 92, 1970, pp. 159-168.

8. Dixon, M. and Probert, S. D., "Heat Transfer Regimes in Vertical, Plane-Walled, Air Filled Cavities". International Journal of Heat and Mass Transfer, Vol. 18, 1975, pp. 709-710.

9. Elder, J. W., "Laminar Free Convection in a Vertical Slot". Journal of Fluid Mechanics, Vol. 23, 1965, p. 77.

10. Emery, A. and Chu, N. C., "Heat Transfer Across Vertical Layers". Journal of Heat Transfer, ASME, Vol. 87, 1965, pp. 110-116.

11. Jakob, M., "Free Heat Convection through Enclosed Plane Gas Layers". Journal of Heat Transfer, ASME, Vol. 68, 1946, pp. 189-194.

12. McAdams, W. H., Heat Transmission, McGraw-Hill Book Co. Inc., 1954.

13. Fishenden, M. and Saunders, O. A., An Introduction to Heat Transfer, Oxford at the Clarendon Press, 1961.

14. Kreith, F., Principles of Heat Transfer, Intext Educational Publishers, 1973.

15. Sparrow, E. M. and Gregg, J. L., "Laminar Free Convection from a Vertical Plate with Uniform Surface Heat Flux", Journal of Heat Transfer, ASME, Vol. 78, 1956, pp. 435-440.

16. Nagendra, H. R., Tirunarayanan, M. A. and Ramachandran, A.,"Laminar Free Convection from Vertical Cylinders with Uniform Heat Flux", Journal of Heat Transfer, ASME, Series C, Vol. 92, 1970, pp. 191-194.

17. Sparrow, E. M. and Gregg, J. L., "Laminar Free Convection Heat Transfer from the Outer Surface of a Vertical Circular Cylinder", Journal of Heat Transfer, ASME, Series C, Vol. 78, 1956. pp. 1823-1829.

18. Gryzagoridis, J., "Leading Edge Effects on the Nusselt Number for a Vertical Plate in Free Convection", International Journal of Heat and Mass Transfer, Vol. 16, 1973, pp. 517-520.

19. Godaux, F. and Gebhart, B., "An Experimental Study of the Transition of Natural Convection Flow Adjacent to a Vertical Surface", International Journal of Heat and Mass Transfer, Vol. 17, 1976, pp. 93-107.

20. Ostrach, S., "An Analysis of Laminar Free Convection Flow and Heat Transfer about a Flat Plate Parallel to the Direction of the Generating Body Force", NACA TR 1111, 1953.

21. Churchill, S. W. and Ozoe, H., "A Correlation for Laminar Free Convection from a Vertical Plate", Journal of Heat Transfer, ASME Vol. 95, 1973, pp. 540-541.

22. Touloukian, Y. S. (Editor) Thermophysical Properties of High Temperature Solid Materials, Vol. 3: Ferrous Alloys. Purdue University Research Centre for Thermophysical Properties, The Macmillan Company, New York. 1967.

23. Wood, W. D., Deem, H. W., Lucks, C. F., "Thermal Radiative Properties", Vol. 3. Plenum Press Handbooks of High Temperature Materials, 1964.

24. Touloukian, Y. S. and Dewitt, D. P., "Thermophysical Properties of Matter", Vol. 7, Thermal Radiative Properties of Metallic Elements and Alloys. IFI/Plenum Press. New York. 1970.

25. Goldsmith, A., Waterman, T. E. and Hirschhorn, H. J., Handbook of Thermophysical Properties of Solid Materials. Vol. 2: Alloys. Macmillan and Co., 1961.

26. Hottel, M. C. and Sarofini, A. F., Radiative Transfer, McGraw-Hill Book Company, 1967.

27. Siegel, R. and Howell, J. R., Thermal Radiation Heat Transfer, McGraw-Hill Book Company, 1972.

28. Dring, R. P. and Gebhart, B., "Hot Wire Anemometer Calibration for Measurements at Very Low Velocity", Journal of Heat Transfer, ASME, Series C. Vol. 91, 1969, pp. 241-244.

29. "Measurements in Low Velocities with Hot Wire Anemometers", Univ. of Minnesota publication.

30. DISA Instruction and Service Manual for Low Velocity Anemometer Type 55D 80/81, DISA Elektronik A/S Herlev, Denmark.

31. DISA Information No. 7, DISA Elektronik A/S Herlev, Denmark, Jan., 1969. pp. 32-35.

32. Manual on the Use of Thermocouples in Temperature Measurement, Special Technical Publication 470, ASTM, Aug. 1970.

33. Gupta, G. K., "Experimental Investigation of Electric Baseboard Heaters", M.Sc. Thesis, The University of Manitoba, 1970.

34. Personal Communication: Dr. D. R. Prowse, Whiteshell Nuclear Research Establishment, Atomic Energy of Canada Limited, Pinawa, Manitoba.

35. Sparrow, E. M., "Laminar Free Convection on a Vertical Plate with Prescribed Non-Uniform Wall Heat Flux or a Prescribed Non-Uniform Wall Temperature", NACA TN 3508, 1955.

36. Fujii, T. and Uehara, H., "Laminar Natural Convective Heat Transfer from the Outer Surface of a Vertical Cylinder", International Journal of Heat and Mass Transfer, V. 13, 1970, pp. 607-615.

37. Gryzagoridis, J., "Combined Free and Forced Convection from an Isothermal Vertical Plate", International Journal of Heat and Mass Transfer, Vol. 18, 1975, pp. 911-916.

38. Vliet, G. C. and Liu, C. K., "An Experimental Study of Turbulent Natural Convection Boundary Layers", Journal of Heat Transfer, ASME, Series C, Vol. 91, 1969, pp. 517-531.

39. Bartalsky, S. L., "Free Convection Heat Transfer on a Vertical Plate under Conditions of Non-Uniform Surface Temperature Distribution", M.Sc. Thesis, Air Force Institute of Technology, Air University, 1958.

40. Hill, R. C., "An Experimental Investigation of Free Convection Heat Transfer from a Non-Isothermal Vertical Flat Plate", M.Sc. Thesis, University of California, Los Angeles, Cal. 1961.

41. Dotson, J. P., "Heat Transfer from a Vertical Plate by Free Convection", M.Sc. Thesis, Purdue University, 1954.

42. Elder, J. W., "Turbulent Free Convection in a Vertical Slot", Journal of Fluid Mechanics, Vol. 23, 1965, p.99.

APPENDIX A

Design and Analysis of Heater

1. Design

Fig. 2 shows the construction details of the heater rod designed jointly by the Department of Mechanical Engineering, University of Manitoba and the Temro Division of James B. Carter Limited of Winnipeg, Manitoba who also built the heater.

The heating element was wound uniformly on a 2" diameter teflon tube threaded to retain the coils in position. The low thermal conductivity of teflon reduced axial heat conduction. The tube was strengthened against buckling by pressing it over an aluminium tube. The maximum power to the heater was restricted by the element temperature to about 550^{o}F beyond which teflon begins to char.

The test surface was made of stainless steel AISI 316 tube with 1/8" wall thickness. Thermocouples to measure the surface temperature were positioned on the inside and the lead wires retained in the grooves of a splined sleeve which was press-fitted inside this tube. The test surface was then finish-ground and polished. The outer tube was centered with respect to the central heater by means of the two end caps also made of steel AISI 316. A mild steel rod was used to retain the two end caps in position, while the spaces between the sleeve and teflon tube as well as that between the central mild steel rod and the aluminium tube were tightly packed with magnesium oxide. This was done to reduce the axial heat conduction.

The locations of the 30 thermocouples are shown in Fig. 2 and their leads were brought equally from the top and bottom face. The leads from the heating element were routed out of the top face.

2. Analysis

The temperature distribution within the heater was obtained using a finite difference approximation. (Refer to Computer Program at the end of this Appendix.) The half cylinder was divided into 21 x 6 subsections and temperatures were computed at 132 nodal points. Free convection from the top, bottom and side surfaces were calculated using empirical relations from McAdams [12]. Radiation losses from the end surfaces were evaluated at the mean temperature of these surfaces while the local wall temperatures were used for the sides. Figs. 8 and 9 each compare the local heat flux values from the numerical analysis with those of the boundary layer measurement. The predictions are within 15 percent of the experimental data.

The heat flux distribution across the heating element shows that less than 10 percent of the total power input flows inward and then flows axially along the aluminium tube and the mild steel rod. This heat flow modifies the expected isothermal situation in the region interior to the heating element and changes the surface heat flux in the end regions. The large deviation of the heat flux in the end region is also due to the heating element not extending to the end of the cylinders. Thus the end caps are mainly heated through conduction by the interior element. Conduction losses also occur along the outer sheath made of stainless steel which contributes to the non-uniform flux in the central region.

The variation in the central region is under 10 percent of the mean and this is entirely due to conduction in the outer sheath. From a manufacturing viewpoint, it was impossible to reduce the thickness of the outer sheath and its variation in the heat flux had to be accepted. The large deviation in the end regions could be substantially reduced if the end caps could be avoided but design considerations prohibit this. An insulator (like teflon) for the end caps might reduce the heat flux variation in the end regions by reducing end losses.

Variables Used in the Fortran Program to Obtain Temperature Distribution in the Vertical Cylinder:

R1	Radius of M.S. rod
R2	Inner radius of aluminium tube
R3	Inner radius of teflon tube
R4	Outer radius of teflon tube
R5	Inner radius of stainless steel tube
R6	Outer radius of cylinder
K1	Thermal conductivity of mild steel
K2	Thermal conductivity of magnesium oxide
K3	Thermal conductivity of aluminium
K4	Thermal conductivity of teflon
K5	Thermal conductivity of stainless steel AISI 316
KA	Thermal conductivity of air
X1	Thickness of end sub-sections
X2	Thickness of interior sub-sections
CHK	Convergence criteria
PR	Prandtl number
GA	Gravitational acceleration
EM	Emissivity of cylinder outer surface
SIGMA	Stefan-Boltzmann constant
TAMB	Ambient temperature
QTH	Total power input
BA	Thermal expansion coefficient
VV	Kinematic viscosity

```
      $JOB    WATFIV      R.SRINIVASAN.
      C---
      C--PROGRAM TO OBTAIN TEMP. DISTRIBUTION IN THE VERTICAL CYLINDER
      C--USING FINITE DIFFERENCE TECHNIQUE.
      C--
 1            DIMENSION T(100,6,2),AH(100),QIN(100),QOUT(100),TCOIL(100),
     1  QSIDE(100),QQSIDE(100)
 2            REAL I,J,K,L,MN,MM,K1,K2,K3,K4,K5,KA
      C--
 3            PRINT 40
 4       40   FORMAT('1',30X,'NODAL TEMP. DISTRIBUTION',40X,'HEAT DIST.',15X,
     1  'SURFACE')
 5            PRINT 50
 6       50   FORMAT(' ',93X,'FROM ELEMENT',14X,'HEAT FLUX')
 7            PRINT 60
 8       60   FORMAT('0','DIST.',9X,'1',10X,'2',10X,'3',10X,'4',7X,'T COIL',
     1  8X,'5',10X,'6',13X,'IN',7X,'OUT')
      C--
 9            PI=3.14159
10            CHK=0.005
      C--
11            X1=.50/12
12            SLABS=19
13            X2=19./SLABS/12
14            N=SLABS+2
      C--
      C   COMPUTE MEAN RADII OF SUB. VOLUMES
      C--
15            R1=3./16/12
16            R1C=R1/2
17            R2=0.5/12
18            R2C=(R2-R1)/2+R1
19            R3=5./8/12
20            R3C=(R3-R2)/2+R2
21            R4=1.0/12
22            R4C=(R4-R3)/2+R3
23            R5=1.375/12
24            R5C=(R5-R4)/2+R4
25            R6=1.625/12
      C--
      C   THERMAL CONDUCTIVITY
      C--
26            K1=26.
27            K2=0.38/1.7303
28            K3=118.
29            K4=0.140
30            K5=8.5
31            KA=0.0154
      C--
32            PR=0.72
33            GA=32.1847
34            SIGMA=.1714*1E-08
35            EM=.29
      C--
36            TAMB=77.0
37            QTH=38.76/0.29307
38            QTHS=QTH/(2*SLABS)
      C--
      C   CONSTANTS FOR SUB VOLUMES
      C--
39            A=(X1*K5)/(1.*ALOG(R2C/R1))
40            B=(R1**2)/(2*(X2/(2*K1)+X1/K5))
41            C=(R1**2)/2
42            D=(X1*K5)/(1.*ALOG(R3C/R2C))
43            CC=(PI*K4*X2)/(ALOG(R4/R4C))
44            DD=(PI*K4*X2)/(ALOG(R5C/R4))


45            E=(R2**2-R1**2)/(2*(X2/(2*K2)+X1/K5))
46            F=(R2**2-R1**2)/2
47            G=(X1*K5)/(1.*ALOG(R4C/R3C))
48            H=(R3**2-R2**2)/(2*(X2/(2*K2)+X1/K5))
49            I=(X1*K5)/(1.*ALOG(R5C/R4C))
50            J=(R3**2-R2**2)/2
51            K=(R4**2-R3**2)/(2*(X2/(2*K4)+X1/K5))
52            L=(R4**2-R3**2)/2
53            AM=(X1*K5)/(1.*ALOG(R6/R5C))
54            NN=(R5**2-R4**2)/(2*(X2/(2*K2)+X1/K5))
55            P=(R5**2-R4**2)/2
56            Q=(R6*X1)
57            R=((R6**2-R5**2)*K5)/(2*(X2/2+X1))
58            S=(R6**2-R5**2)/2
59            TT=(R1**2*K1)/(2*X2)
```

```
60          U=((R2**2-R1**2)*K2)/(2*X2)
61          V=((R3**2-R2**2)*K3)/(2*X2)
62          W=((R4**2-R3**2)*K4)/(2*X2)
63          X=((R5**2-R4**2)*K2)/(2*X2)
64          Y=((R6**2-R5**2)*K5)/(2*X2)
65          AA=(X2*K2)/(ALOG(R2C/R1))
66          BB=X2/(1.*((ALOG(R2/R2C))/K2+(ALOG(R3C/R2))/K3))
67          GG=X2/(1.*((ALOG(R3/R3C))/K3+(ALOG(R4C/R3))/K4))
68          MM=X2/(1.*((ALOG(R5/R5C))/K2+(ALOG(R6/R5))/K5))
69          QO=R6*X2
      C--
      C   INITIAL TEMPERATURE DISTRIBUTION
      C--
70          TEMP=125.
71          DO 2 M=1,N
72          DO 3 II=1,6
73        3 T(M,II,1)=TEMP
74        2 TEMP=TEMP-0.8
75      150 CONTINUE
      C--
      C   COMBINED CONV. & RAD. COEFF. FOR TOP & BOTTOM SURFACE
      C--
76       15 HT=0.27*((ABS(T(1,4,1)-TAMB))/(0.9*2*R6))**0.25
         1 +SIGMA*EM*((T(1,4,1)+460)**4-(TAMB+460)**4)/(ABS(T(1,4,1)-TAMB))
77          HB=0.12*((ABS(T(N,4,1)-TAMB))/(0.9*2*R6))**0.25
          1 +SIGMA*EM*((T(N,4,1)+460)**4-(TAMB+460)**4)/(ABS(T(N,4,1)-TAMB))
      C--
78          DIST=19./12.
79          DO 5 M=1,N
80          TMEAN=(ABS(T(M,6,1)+TAMB))/2.
81          BA=1./(TMEAN+460)
82          VV=(.647+.044/20*(TMEAN-100.))/3600.
83          IF(TMEAN.GT.100) GO TO 345
84          VV=(.607+.04/20*(TMEAN-80.))/3600.
85       345 AB=.41*KA*(PR*GA*BA/VV**2)**0.25
86          IF(M.EQ.1) GO TO 6
87          IF(M.EQ.N) GO TO 9
      C--
      C   COMBINED CONV. & RAD. COEFF. FOR THE SIDE SURFACE
      C--
88          AH(M)=AB*((ABS(T(M,6,1)-TAMB))/DIST)**.25+SIGMA*EM*((T(M,6,1)+
          1 460)**4-(TAMB+460)**4)/((ABS(T(M,6,1)-TAMB)))
      C--
89          DIST=DIST-X2
90          TCOIL(M)=(QTHS+CC*T(M,4,1)+DD*T(M,5,1))/(CC+DD)
91          QIN(M)=CC*(TCOIL(M)-T(M,4,1))
92          QOUT(M)=DD*(TCOIL(M)-T(M,5,1))
93       45 CONTINUE
94          IF (M.EQ.2) GO TO 7
95          IF (M.EQ.(N-1)) GO TO 8
96          GO TO 10


      C--
      C   CALCULATE NODAL POINT TEMPS.
      C--
97        6 CONTINUE
98          QIN(M)=0.
99          QOUT(M)=0.
100         TCOIL(M)=0.
101         AH(M)=AB*((ABS(T(M,6,1)-TAMB))/(19.75/12))**0.25
          1+SIGMA*EM*((T(M,6,1)+460)**4-(TAMB+460)**4)/(ABS(T(M,6,1)-TAMB))
102         T(M,1,2)=(2*A*T(M,2,1)+B*T(M+1,1,1)+C*HT*TAMB)/(2*A+B+C*HT)
103         T(M,2,2)=(A*T(M,1,2)+D*T(M,3,1)+E*T(M+1,2,1)+F*HT*TAMB)/
          1 (A+D+E+F*HT)
104         T(M,3,2)=(D*T(M,2,2)+G*T(M,4,1)+H*T(M+1,3,1)+J*TAMB*HT)/
          1(D+G+H+J*HT)
105         T(M,4,2)=(G*T(M,3,2)+I*T(M,5,1)+K*T(M+1,4,1)+L*TAMB*HT)/
          1 (G+I+K+L*HT)
106         T(M,5,2)=(I*T(M,4,2)+AM*T(M,6,1)+NN*T(M+1,5,1)+P*TAMB*HT)/
          1 (I+AM+NN+P*HT)
107         T(M,6,2)=(AM*T(M,5,2)+R*T(M+1,6,1)+S*HT*TAMB+Q*AH(M)*TAMB)/
          1 (AM+R+S*HT+Q*AH(M))
108         GO TO 5
```

```
      C
109         7  CONTINUE
110              T(M,1,2)=(B*T(M-1,1,2)+AA*2*T(M,2,1)+TT*T(M+1,1,1))/(B+2*AA+TT)
111              T(M,2,2)=(AA*T(M,1,2)+U*T(M+1,2,1)+BB*T(M,3,1)+E*T(M-1,2,2))/
             1  (AA+U+BB+E)
112              T(M,3,2)=(BB*T(M,2,2)+GG*T(M,4,1)+H*T(M-1,3,2)+V*T(M+1,3,1))/
             1  (BB+GG+H+V)
113              T(M,4,2)=(GG*T(M,3,2)+K*T(M-1,4,2)+W*T(M+1,4,1)+
             1  QIN(M)/PI)/(GG+K+W)
114              T(M,5,2)=(MM*T(M,6,1)+X*T(M+1,5,1)+NN*T(M-1,5,2)+
             1  QOUT(M)/PI)/(MM+X+NN)
115              T(M,6,2)=(MM*T(M,5,2)+Y*T(M+1,6,1)+R*T(M-1,6,2)+AH(M)*TAMB*QQ)/
             1  (MM+Y+R+AH(M)*QQ)
116              GO TO 5
      C
117        10  CONTINUE
118              T(M,1,2)=(TT*T(M-1,1,2)+TT*T(M+1,1,1)+AA*2*T(M,2,1))/(TT*2+AA*2)
119              T(M,2,2)=(AA*T(M,1,2)+U*T(M-1,2,2)+BB*T(M,3,1)+U*T(M+1,2,1))/
             1  (AA+BB+2*U)
120              T(M,3,2)=(BB*T(M,2,2)+GG*T(M,4,1)+V*T(M-1,3,2)+V*T(M+1,3,1))
             1  /(BB+GG+2*V)
121              T(M,4,2)=(GG*T(M,3,2)+W*T(M-1,4,2)+W*T(M+1,4,1)+
             1  QIN(M)/PI)/(GG+2*W)
122              T(M,5,2)=(MM*T(M,6,1)+X*T(M-1,5,2)+X*T(M+1,5,1)+
             1  QOUT(M)/PI)/(MM+2*X)
123              T(M,6,2)=(MM*T(M,5,2)+Y*T(M-1,6,2)+Y*T(M+1,6,1)+AH(M)*TAMB*QQ)/
             1  (MM+2*Y+AH(M)*QQ)
124              GO TO 5
      C
125         8  CONTINUE
126              T(M,1,2)=(B*T(M+1,1,1)+AA*2*T(M,2,1)+TT*T(M-1,1,2))/(B+2*AA+TT)
127              T(M,2,2)=(AA*T(M,1,2)+U*T(M-1,2,2)+BB*T(M,3,1)+E*T(M+1,2,1))/
             1  (AA+U+BB+E)
128              T(M,3,2)=(BB*T(M,2,2)+GG*T(M,4,1)+H*T(M+1,3,1)+V*T(M-1,3,2))/
             1  (BB+GG+H+V)
129              T(M,4,2)=(GG*T(M,3,2)+K*T(M+1,4,1)+W*T(M-1,4,2)+
             1  QIN(M)/PI)/(GG+K+W)
130              T(M,5,2)=(MM*T(M,6,1)+X*T(M-1,5,2)+NN*T(M+1,5,1)+
             1  QOUT(M)/PI)/(MM+X+NN)
131              T(M,6,2)=(MM*T(M,5,2)+Y*T(M-1,6,2)+R*T(M+1,6,1)+AH(M)*TAMB*QQ)/
             1  (MM+Y+R+AH(M)*QQ)
132              GO TO 5
      C
133         9  CONTINUE
134              QIN(M)=0.

135              QOUT(M)=0.
136              TCOIL(M)=0.
137              AH(M)=AB*((ABS(T(M,6,1)-TAMB))/(0.25/12))**0.25
             1+SIGMA*EM*((T(M,6,1)+460)**4-(TAMB+460)**4)/(ABS(T(M,6,1)-TAMB))
138               T(M,1,2)=(2*A*T(M,2,1)+B*T(M-1,1,2)+C*HB*TAMB)/(2*A+B+C*HB)
139              T(M,2,2)=(A*T(M,1,2)+D*T(M,3,1)+E*T(M-1,2,2)+F*HB*TAMB)/
             1  (A+D+E+F*HB)
140              T(M,3,2)=(D*T(M,2,2)+G*T(M,4,1)+H*T(M-1,3,2)+J*TAMB*HB)/
             1(D+G+H+J*HB)
141              T(M,4,2)=(G*T(M,3,2)+I*T(M,5,1)+K*T(M-1,4,2)+L*TAMB*HB)/
             1  (G+I+K+L*HB)
142              T(M,5,2)=(I*T(M,4,2)+AM*T(M,6,1)+NN*T(M-1,5,2)+P*TAMB*HB)/
             1  (I+AM+NN+P*HB)
143              T(M,6,2)=(AM*T(M,5,2)+R*T(M-1,6,2)+S*HB*TAMB+Q*AH(M)*TAMB)/
             1  (AM+R+S*HB+Q*AH(M))
144         5  CONTINUE
      C--
      C  CALCULATE ABS. DIFFERENCE BETWEEN OLD & NEW TEMP. AT EACH NODE
      C--
145              DET=0
146              DO 20 M=1,N
147              DO 20 II=1,6
148              DT=ABS(T(M,II,2)-T(M,II,1))
149              IF (DT.LE.DET) GO TO 20
150              DET=DT
151        20  CONTINUE
```

```
C--
C  CHECK MAX. TEMP. DIFF. WITH CONV. CRITERIA
C--
152         IF(DET.LE.CHK) GO TO 120
C--
C  REPLACE OLD VALUES OF TEMP. WITH NEW VALUES
C--
153         DO 140 M=1,N
154         DO 140 II=1,6
155   140   T(M,II,1)=T(M,II,2)
156         GO TO 150
157   120   CONTINUE
C--
C  CALCULATE HEAT LOSS FROM TOP & BOTTOM FACE
C--
158         QSURFT=HT*PI*R6**2/2*(T(1,4,2)-TAMB)
159         QSURFB=HB*PI*R6**2/2*(T(N,4,2)-TAMB)
C--
C  CALCULATE CONV. HEAT LOSS FROM SIDE FACE
C--
160         AH(1)=AH(1)
          1-SIGMA*EM*((T(1,6,2)+460)**4-(TAMB+460)**4)/(ABS(T(1,6,2)-TAMB))
161         QSIDE(1)=AH(1)*PI*R6*X1*(T(1,6,2)-TAMB)
162         QQSIDE(1)=2*QSIDE(1)*144./(PI*3.25*0.5)
163         AH(N)=AH(N)
          1-SIGMA*EM*((T(N,6,2)+460)**4-(TAMB+460)**4)/(ABS(T(N,6,2)-TAMB))
164         QSIDE(N)=AH(N)*PI*R6*X1*(T(N,6,2)-TAMB)
165         QQSIDE(N)=2*QSIDE(N)*144./(PI*3.25*0.5)
166         QSUM=QSIDE(1)+QSIDE(N)
167         NS=SLABS+1
168         DO 4 M=2,NS
169         AH(M)=AH(M)
          1-SIGMA*EM*((T(M,6,2)+460)**4-(TAMB+460)**4)/(ABS(T(M,6,2)-TAMB))
170         QSIDE(M)=AH(M)*PI*R6*X2*(T(M,6,2)-TAMB)
171         QQSIDE(M)=2*QSIDE(M)*144./(PI*3.25)
C--
C  CALCULATE TOTAL CONV. HEAT LOSS FROM SIDE FACE
C--
172         QSUM=QSUM+QSIDE(M)
173         QQSUM=2*QSUM

174       4 CONTINUE
C--
175         DO 180 M=1,N
176         JN=N-M
177         PRINT 160,JN,(T(M,II,2),II=1,4),TCOIL(M),(T(M,II,2),II=5,6),
          1 QIN(M),QOUT(M),QQSIDE(M)
178   160   FORMAT(' ',I4,2X,7F11.2,F14.2,F9.2,F19.2)
179   180   CONTINUE
C--
180         PRINT 90
181    90   FORMAT('-',5X,'TOTAL POWER INPUT',10X,'CONV. FROM SIDE',10X,'TOP
          1 LOSS',10X,'BOTTOM LOSS')
182         PRINT 100,QTH,QQSUM,QSURFT,QSURFB
183   100   FORMAT(' ', 7X,F6.2,' BTU/HR',13X,F6.2,' BTU/HR', 9X,F6.2,
          1 'BTU/HR', 8X,F6.2,'BTU/HR')
184         STOP
185         END

$ENTRY
```

NODAL TEMP. DISTRIBUTION

DIST.	1	2	3	4	T COIL	5	6	HEAT DIST. FROM ELEMENT IN	HEAT DIST. FROM ELEMENT OUT	SURFACE HEAT FLUX
20	152.46	152.17	151.93	151.74	0.00	151.62	151.69	0.00	0.00	39.96
19	171.81	174.94	176.55	176.36	177.45	162.04	154.54	0.19	3.29	42.15
18	176.39	177.98	179.04	180.08	181.06	165.57	157.01	0.17	3.31	44.33
17	178.46	179.12	179.56	181.18	182.49	167.26	158.78	0.23	3.25	46.12
16	179.49	179.79	180.00	181.90	183.42	168.37	159.97	0.27	3.21	47.62
15	180.05	180.22	180.34	182.39	184.02	169.06	160.71	0.29	3.19	48.91
14	180.39	180.47	180.56	182.67	184.36	169.44	161.10	0.30	3.18	50.03
13	180.48	180.58	180.65	182.77	184.46	169.54	161.21	0.30	3.18	51.04
12	180.47	180.56	180.62	182.71	184.36	169.42	161.07	0.29	3.19	51.97
11	180.32	180.41	180.47	182.48	184.08	169.09	160.71	0.28	3.20	52.85
10	180.02	180.13	180.19	182.11	183.62	168.57	160.15	0.27	3.21	53.70
9	179.67	179.75	179.80	181.59	183.01	167.87	159.41	0.25	3.23	54.56
8	179.18	179.25	179.31	180.94	182.23	166.99	158.48	0.23	3.25	55.45
7	178.59	178.66	178.72	180.16	181.30	165.93	157.35	0.20	3.28	56.40
6	177.89	177.98	178.04	179.24	180.20	164.68	156.00	0.17	3.31	57.48
5	177.07	177.20	177.30	178.20	178.93	163.21	154.43	0.13	3.35	58.76
4	176.04	176.22	176.30	177.04	177.48	161.52	152.61	0.08	3.40	60.42
3	174.58	174.75	175.70	175.77	175.83	159.57	150.50	0.01	3.47	62.80
2	172.05	173.77	174.32	174.27	173.91	157.29	148.09	-0.09	3.54	66.54
1	168.81	170.26	174.27	170.25	170.08	153.62	145.46	-0.03	3.51	70.03
0	145.08	144.74	144.39	144.08	0.00	143.71	143.41	0.00	0.00	133.74

TOTAL POWER INPUT 132.26 BTU/HR CONV. FROM SIDE 78.66 BTU/HR TOP LOSS 3.25BTU/HR BOTTOM LOSS 1.66BTU/HR

CORE USAGE OBJECT CODE= 17480 BYTES, ARRAY AREA= 7200 BYTES, TOTAL AREA AVAILABLE= 61440 BYTES

DIAGNOSTICS NUMBER OF ERRORS= 0, NUMBER OF WARNINGS= 0, NUMBER OF EXTENSIONS= 0

COMPILE TIME= 0.42 SEC, EXECUTION TIME= 19.70 SEC, 13.17.03 WEDNESDAY 27 JUL 77 WATFIV - JAN 1970 V1L5

C$STOP

NUDAL TEMP. DISTRIBUTION

DIST.	1	2	3	4	T COIL	5	6	HEAT DIST. FROM ELEMENT IN	HEAT DIST. FROM ELEMENT OUT	SURFACE HEAT FLUX
20	117.96	117.82	117.71	117.63	0.00	117.58	117.61	0.00	0.00	18.48
19	128.91	128.36	130.24	129.06	129.60	122.43	118.94	0.10	1.53	19.42
18	129.03	129.77	130.27	130.80	131.29	124.08	120.11	0.09	1.54	20.37
17	129.99	130.30	130.51	131.32	131.97	124.88	120.94	0.12	1.51	21.17
16	130.40	130.01	130.74	131.00	132.41	125.41	121.51	0.13	1.49	21.84
15	130.72	130.84	130.87	131.88	132.69	125.74	121.87	0.14	1.48	22.41
14	130.88	130.92	130.97	132.02	132.85	125.92	122.05	0.15	1.48	22.92
13	130.92	130.97	131.01	132.06	132.90	125.97	122.10	0.15	1.48	23.38
12	130.90	130.95	130.99	132.02	132.89	125.91	122.03	0.15	1.48	23.81
11	130.83	130.87	130.91	131.91	132.71	125.75	121.86	0.14	1.49	24.22
10	130.69	130.74	130.77	131.73	132.48	125.49	121.58	0.13	1.49	24.61
9	130.51	130.55	130.58	131.47	132.18	125.15	121.22	0.13	1.50	25.01
8	130.27	130.31	130.34	131.13	131.80	124.72	120.76	0.11	1.51	25.43
7	129.98	130.02	130.05	130.77	131.34	124.20	120.20	0.10	1.52	25.87
6	129.65	129.69	129.73	130.33	130.81	123.58	119.52	0.08	1.54	26.38
5	129.25	129.32	129.37	129.83	130.19	122.87	118.78	0.06	1.56	26.99
4	128.78	128.90	128.99	129.27	129.48	122.05	117.89	0.04	1.59	27.76
3	128.27	128.39	128.51	128.65	128.69	121.10	116.87	0.01	1.62	28.92
2	127.88	127.89	128.24	127.93	127.76	120.01	115.71	-0.03	1.66	30.84
1	124.42	126.05	127.93	126.04	125.95	118.26	114.45	-0.02	1.64	35.17
0	114.22	114.07	113.91	113.77	0.00	113.60	113.47	0.00	0.00	48.10

TOTAL POWER INPUT 61.79 BTU/HR CONV. FROM SIDE 36.15 BTU/HR TOP LOSS 1.488TU/HR BUTTOM LOSS 0.778TU/HR

CORE USAGE OBJECT CODE= 17480 BYTES, ARRAY AREA= 7200 BYTES, TOTAL AREA AVAILABLE= 61440 BYTES

DIAGNOSTICS NUMBER OF ERRORS= 0, NUMBER OF WARNINGS= 0, NUMBER OF EXTENSIONS= 0

COMPILE TIME= 0.43 SEC, EXECUTION TIME= 42.52 SEC, 9.32.33 MONDAY 8 AUG 77 WATFIV - JAN 1976 V1L5

CSSTOP

APPENDIX B

1. Calibration of the Low Velocity Anemometer

Anemometers can be calibrated either by placing the probe in a flow of predetermined velocity or by moving the probe at a constant speed through a stationary fluid. This latter method has been explained by Dring and Gebhart [28]. The low velocity anemometer was calibrated by the conventional method of producing a constant velocity flow as a portion of the calibration equipment used by Gupta [33] was available.

The DISA manual for the low velocity anemometer [30] mentions a built-in calibration facilty to permit correction for various parameters including the gas temperature. It also implied that the ratio of the first two harmonics of the output signal was independent of gas temperature level. Experiments showed temperature dependences for both approaches. Hence the probe had to be calibrated at different flow temperatures.

Fig. 26 shows the set-up for calibration. Air, displaced from a glass flask by inflowing water, was fed into an 8-mm diameter tube. The water flow rate was maintained constant by avoiding any pressure head variations at the inlet to the flask. The displaced air was passed through an 8-mm tube, a portion of which was heated by coils wound around the tube and enclosed in a can. The tube length beyond the can was sufficient to ensure a fully developed laminar flow. Different calibration temperatures were obtained by varying the voltage impressed across the heater coils. A continuously variable transformer 0-120 V was used for this purpose.

The calibration was carried out in a closed chamber thus avoiding the affects of stray currents on the flow rate. The flow rate was obtained by noting the time required for a fixed volume of water to fill in the flask. The air temperature was measured with an iron-constantan thermocouple referenced to an ice bath and the output from the low velocity anemometer was read on a DISA digital voltmeter, Type 55D31.

Assuming a parabolic velocity profile, the peak velocity as read by the probe was twice the mean velocity of the flow. As mentioned in DISA information No. 7 [31] the calibration curves shown in Fig. 27 show a linear range up to approximately 20 cm/sec.

2. Thermocouple Calibration

Type J (Iron +, constantan -) thermocouples were calibrated by the comparison method described in the ASTM manual on the use of thermocouples [32]. The reference temperature used was an ice bath while the calibration temperature was obtained through a constant temperature circulator, Type F423, from Haake Inc., Germany. Bath temperatures were read to within 0.2 F^{o} on a precision thermometer.

APPENDIX C

SAMPLE CALCULATIONS

1. Emmissivity of the Heater Surface:

Power input to the heater = 18.11 watts = 61.8 Btu/hr.

Temperature of top surface = $119^{o}F$

Ambient temperature = $78.4^{o}F$

$h_{conv.}$ for top surface = $0.27\ (\frac{\Delta T}{D})^{1/4}$

= $0.963\ Btu/hr.ft^{2}.F^{o}$

$\therefore$ losses from top surface =

Convection = 1.95 Btu/hr.

Radiation = 0.74 Btu/hr. ($\varepsilon = 0.30$ assumed)

Heat loss from bottom surface assumed nil as the heater rests on an insulator

Average surface heat flux from Fig. 8 = 27.5 Btu/hr.sq.ft.

$\therefore$ convective heat loss from sides = 39.0 Btu/hr.

$\therefore$ heat lost by radiation from side = 61.8 - (1.95 + 0.74 + 39.0)

= 20.11 Btu/hr.

$$q_{rad.} = \varepsilon\ \sigma\ \Sigma\ A_{w}(T_{w}^{4} - T_{\infty}^{4})$$

$$\therefore \varepsilon = \frac{20.11}{0.1714 \times 10^{-8}\ \Sigma\ A_{w}(T_{w}^{4} - T_{\infty}^{4})}$$

$$= 0.291.$$

2. Unbounded Free Convection:

2.1 Local Nusselt and Grashof Number:

Power input = 18.11 watts

At 6.0" from leading edge:

Local heat flux = 27.0 Btu/hr-ft^2

Wall temperature = 118.7^{o}F

Ambient temperature = 78.4^{o}F

Mean temperature = 98.4^{o}F

Properties of air evaluated at mean temperature:

Density of dry air (ρ_a) = 0.0712 lbm/ft^2

Thermal conductivity = K_a = 0.01535 Btu/hr-ft-^{o}F (Ref. [14])

Atmospheric pressure = 14.2836 psia

Wet bulb temperature = 54^{o}F

$$\text{Vapour pressure} = p' - \frac{(p_{atm} - p')(T_1 - T_2)}{(2831 \times 1.43 \times T_2)}$$

T_1 and T_2 = dry and wet bulb temp. respectively

p' = saturation pressure at T_2 ^{o}F

p_{atm} = atmospheric pressure

$\therefore$ Vapour pressure = 0.0939 psi.

$$\text{Density of air vapour mixture} = \rho_a\left(1 - 0.378 \frac{p_v}{p_{atm}}\right)$$

$$= 0.0710 \text{ lbm/ft}^3$$

μ_{air} = 1.275 x 10^{-5} lbm/sec.ft

ν_{air} = 1.7958 x 10^{-4} ft^2/sec

g at Winnipeg = 32.1847 ft/sec^2

$$Gr_x^* = \left(\frac{g\beta}{\nu^2}\right)\left(\frac{q}{K}\right) x^4$$

$$= (1.788 \times 10^6)\left(\frac{q}{K}\right) x^4$$

$$= 1.967 \times 10^8$$

$$Nu_x = \frac{h\,x}{K}$$

at the wall, $q = -K\left(\frac{dT}{dy}\right)_w = h\,(T_w - T_\infty)$

$$\therefore \quad (h/K) = -\frac{(dT/dy)_w}{\Delta T}$$

$$\therefore \quad Nu_x = 21.2$$

2.2 Average Nusselt and Grashof Number:

(i) Based on Cylinder Height:

Power input = 18.11 watts

Average surface heat flux = 27.5 Btu/hr.sq.ft.

Average wall temperature = 119^oF

Ambient temperature = 78.4^oF

with properties evaluated at the mean temperature,

$$Nu_H = \frac{qH}{K\Delta T} = 73.5$$

$$Gr_H = \left(\frac{g\beta}{\nu^2}\right)(\Delta T)\, H^3 = 3.381 \times 10^8$$

$$\therefore \quad Nu_H = 0.588\,(Ra_H)^{1/4}$$

Similarly, for power input of 38.61 watts

$$Nu_H = 0.564\,(Ra_H)^{1/4}$$

(ii) Based on diameter:

$$Nu_D = \frac{qD}{K\Delta T}$$

$$Gr_D = \left(\frac{g\beta}{\nu^2}\right)(\Delta T)\, D^3$$

The corresponding expressions are:

$$Nu_D = 0.588\ (Ra_D \frac{D}{H})^{1/4} \quad \text{for } Q = 18.11 \text{ watts}$$

$$= 0.564\ (Ra_D \frac{D}{H})^{1/4} \quad \text{for } Q = 38.61 \text{ watts}$$

3. Vertical Annuli:

3.1 Local Nusselt and Grashof Number:

Power input = 18.11 watts

At 9" from bottom face:

Local wall temperature = 121.8^oF

Outer wall temperature = 66^oF

Local heat flux from wall temperature gradient = 24.31 $Btu/hr.ft^2$

Properties evaluated at mean temperature = 93.9^oF

$$Nu_x = \frac{h_x\, x}{K} = \frac{(dT/dy)_w}{\Delta T}\,(x)$$

$$= 21.27$$

$$Gr_x^* = \left(\frac{g\beta}{\nu^2}\right)\left(\frac{q}{K}\right) x^4$$

$$= 9.394 \times 10^8$$

3.2 Overall Heat Transfer: based on gap width:

Power input = 18.11 watts = 61.8 Btu/hr

Heat loss from top face: Convection = 2.14 Btu/hr

Radiation = 0.77 Btu/hr

Radiation loss from the side:

Radiant heat exchange between two cylindrical surfaces is expressed as:

$$q_{1-2} = \frac{A_1 \ (T_1^4 - T_2^4)}{\frac{1}{\varepsilon_1} + (\frac{1}{\varepsilon_2} - 1) \frac{A_1}{A_2}}$$

A_1 and A_2 - Surface areas of inner and outer cylinder

ε_1 and ε_2 - Emmissivity of the surfaces.

As shown earlier, ε for the heater surface = 0.29

and ε for carbon steel = 0.80 (assumed)

Average hot wall temperature = $119.4^{o}F$

cold wall temperature = $66^{o}F$

$$\therefore q_{1-2} = 24.22 \text{ Btu/hr.}$$

$\therefore$ net heat convected = 61.8 - (24.22 + 2.14 + 0.77)

= 34.67 Btu/hr.

$$\therefore Nu_W = \frac{qW}{K\Delta T} = 1.87$$

$$Gr_W = (\frac{g\beta}{\nu^2})(\Delta T) \ W^3 = 2.461 \times 10^4$$

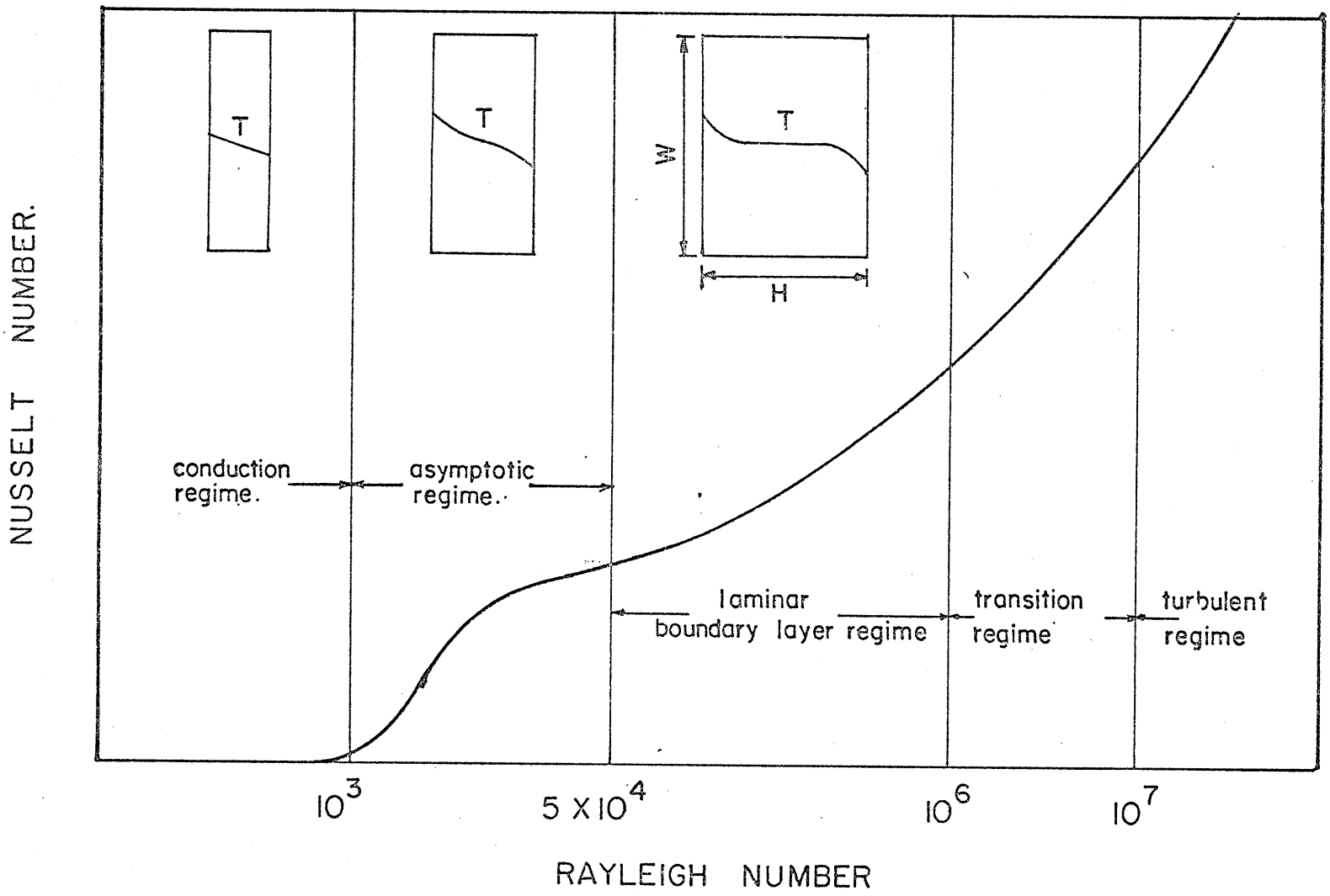

Fig.I. Sketch Showing Different Flow Regimes in Vertical Convection Layers.

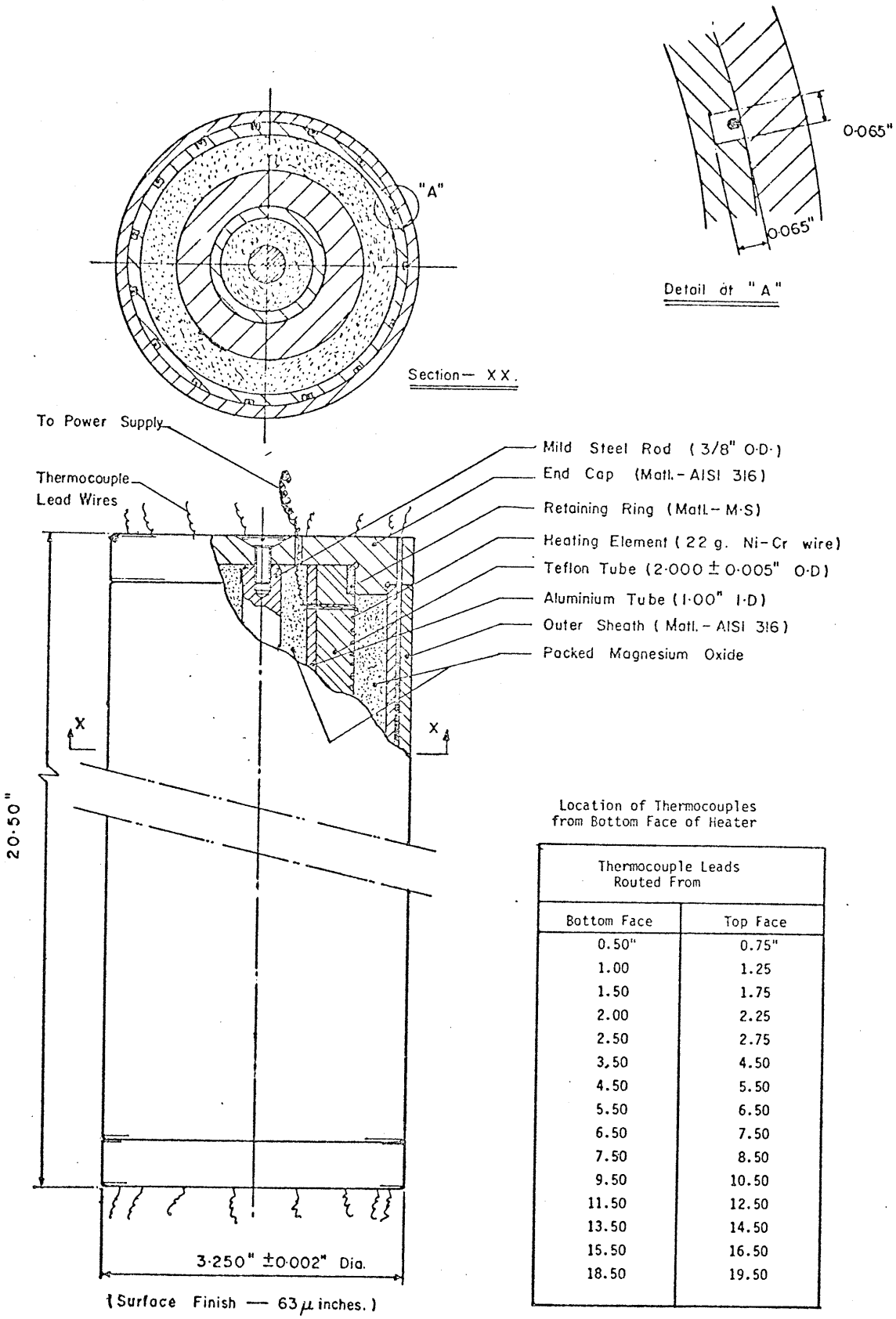

Location of Thermocouples from Bottom Face of Heater

Thermocouple Leads Routed From	
Bottom Face	Top Face
0.50"	0.75"
1.00	1.25
1.50	1.75
2.00	2.25
2.50	2.75
3.50	4.50
4.50	5.50
5.50	6.50
6.50	7.50
7.50	8.50
9.50	10.50
11.50	12.50
13.50	14.50
15.50	16.50
18.50	19.50

Fig. 2. Details of Heater.

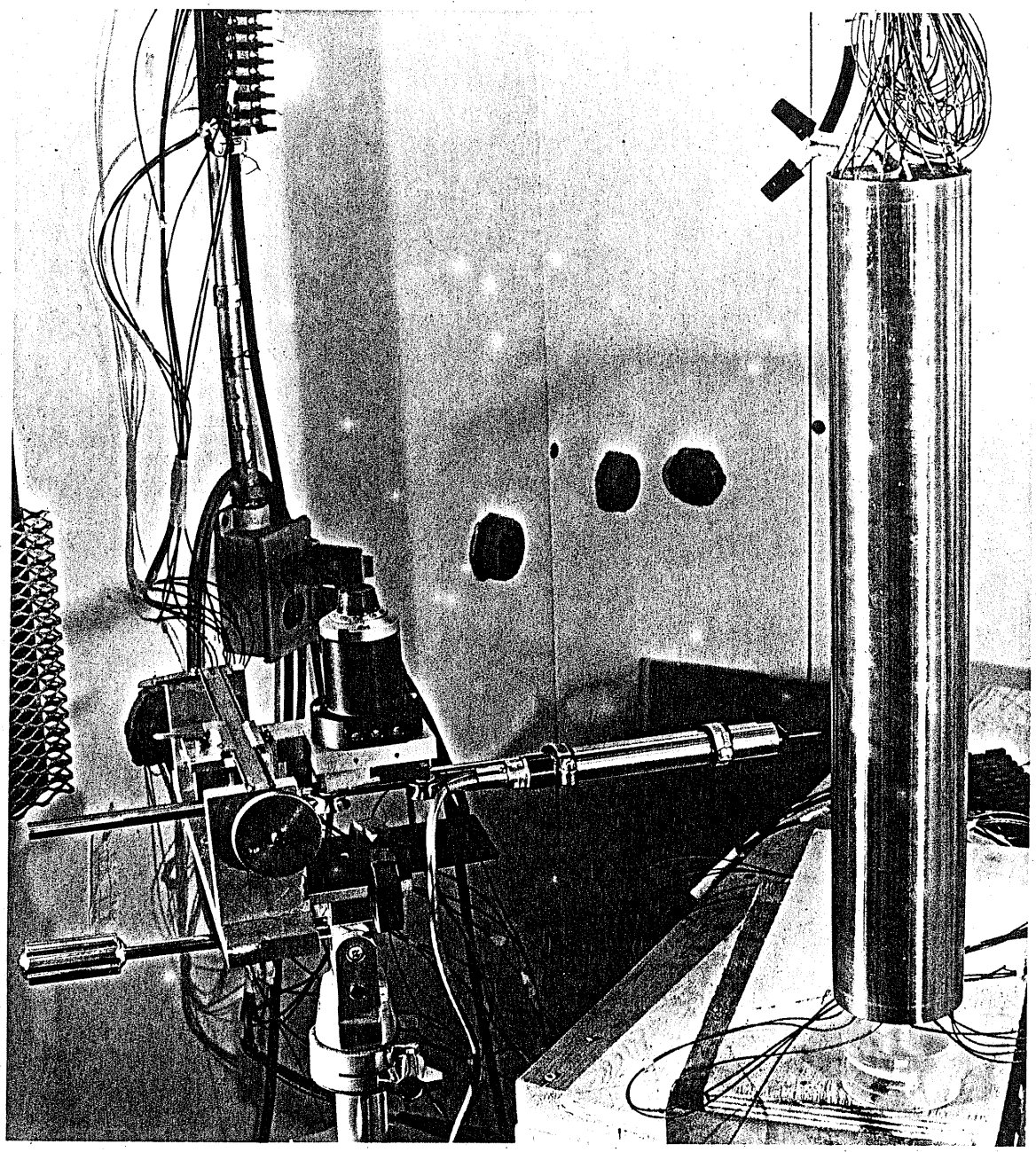

Fig. 3 Traversing Mechanism with Velocity Probe.

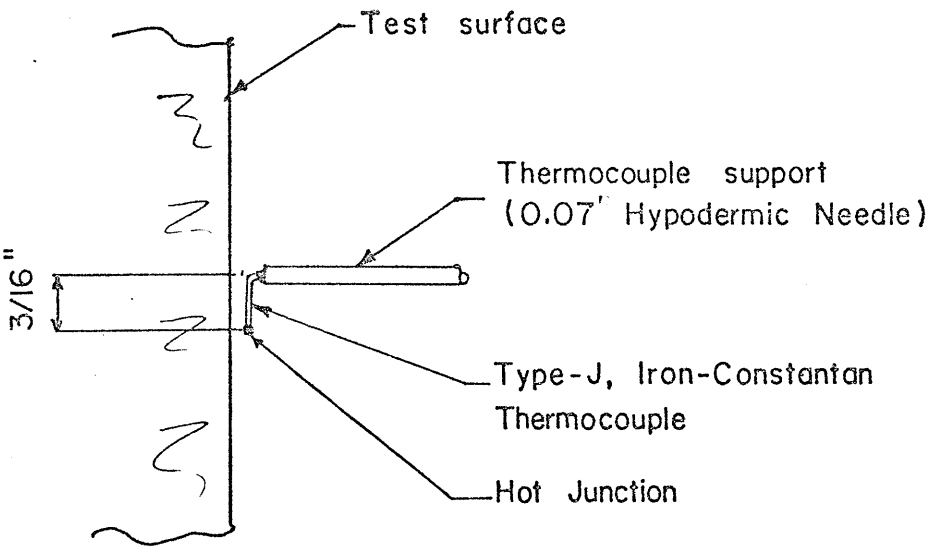

Fig. 4. Temperature Probe.

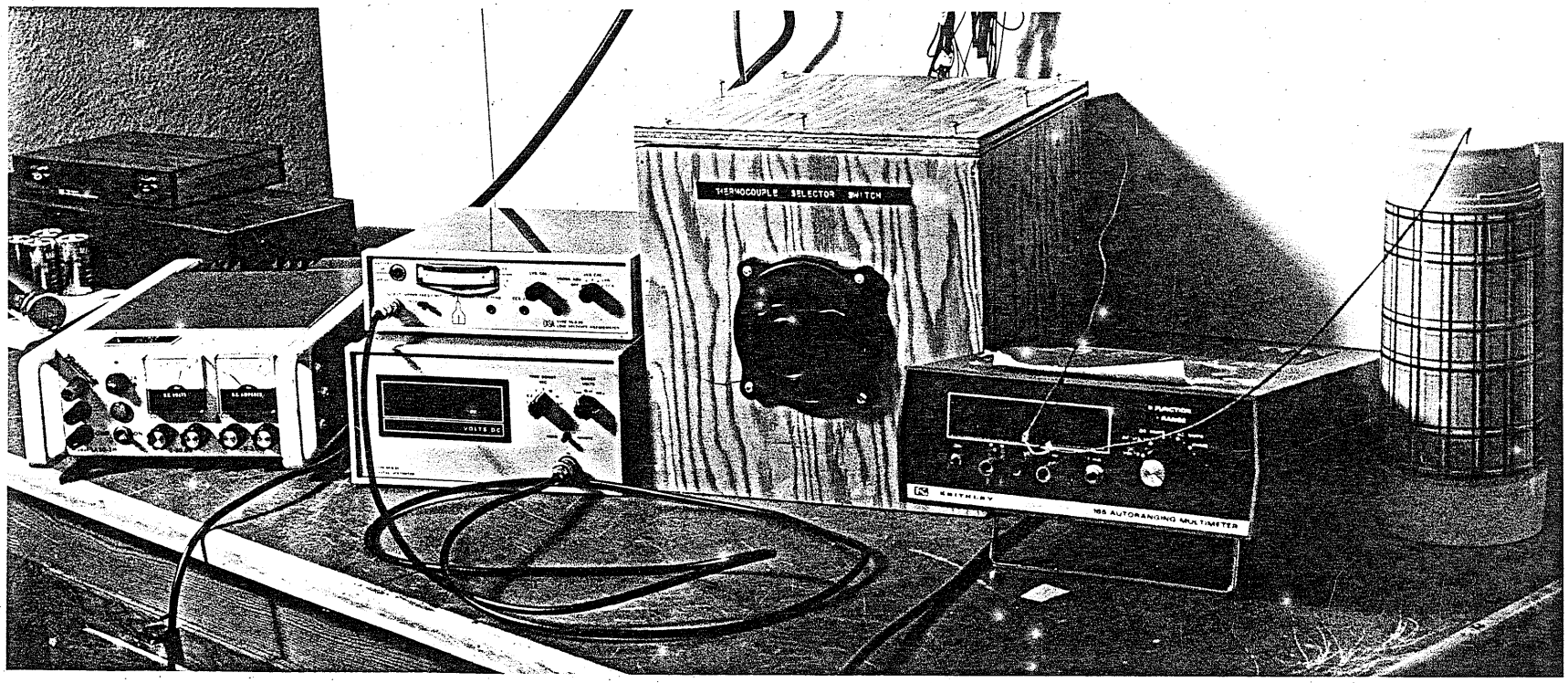

Fig. 5 Instruments Used for This Investigation.

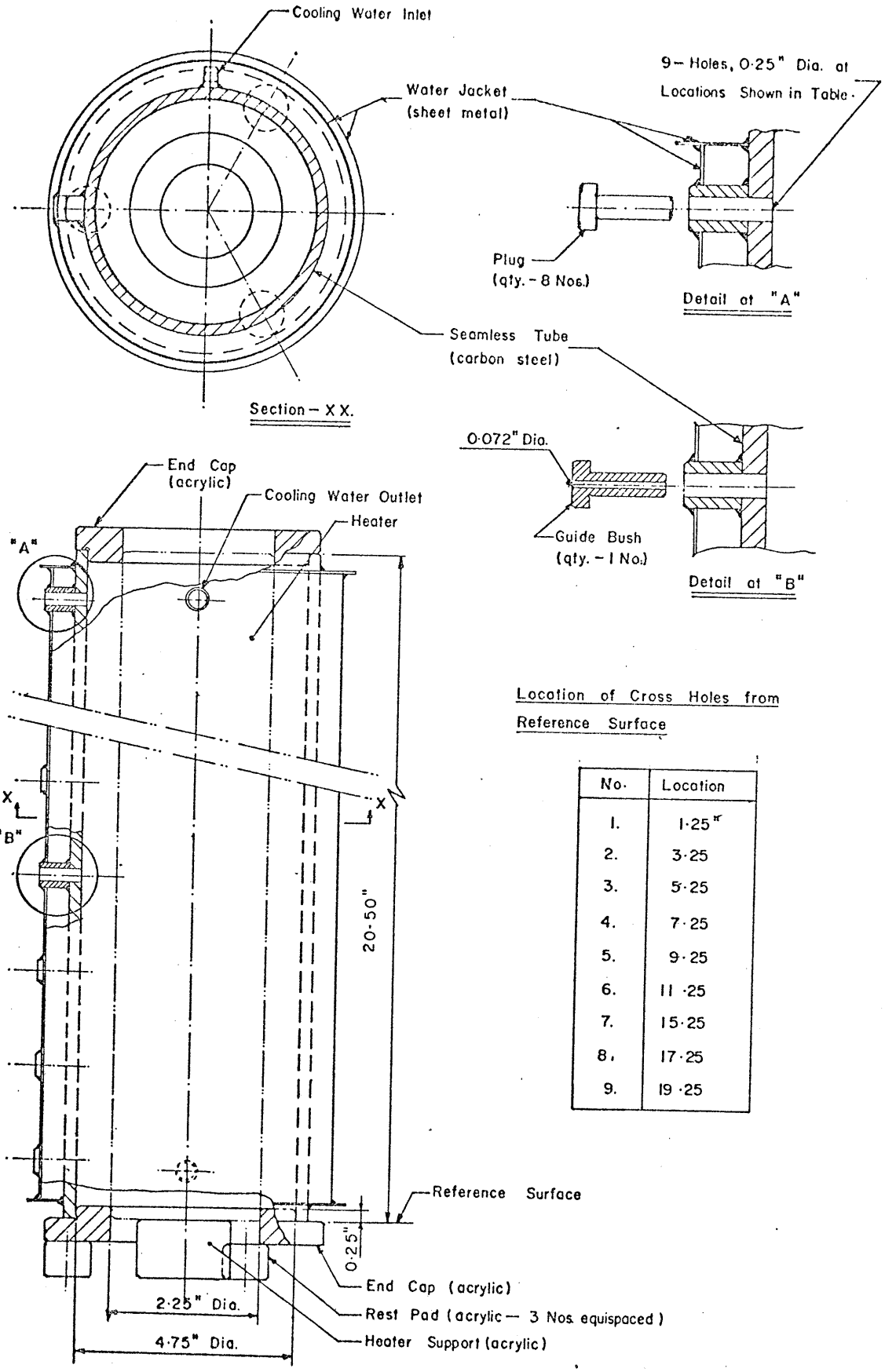

Location of Cross Holes from Reference Surface

No.	Location
1.	1·25"
2.	3·25
3.	5·25
4.	7·25
5.	9·25
6.	11·25
7.	15·25
8.	17·25
9.	19·25

Fig. 6 Details of Can.

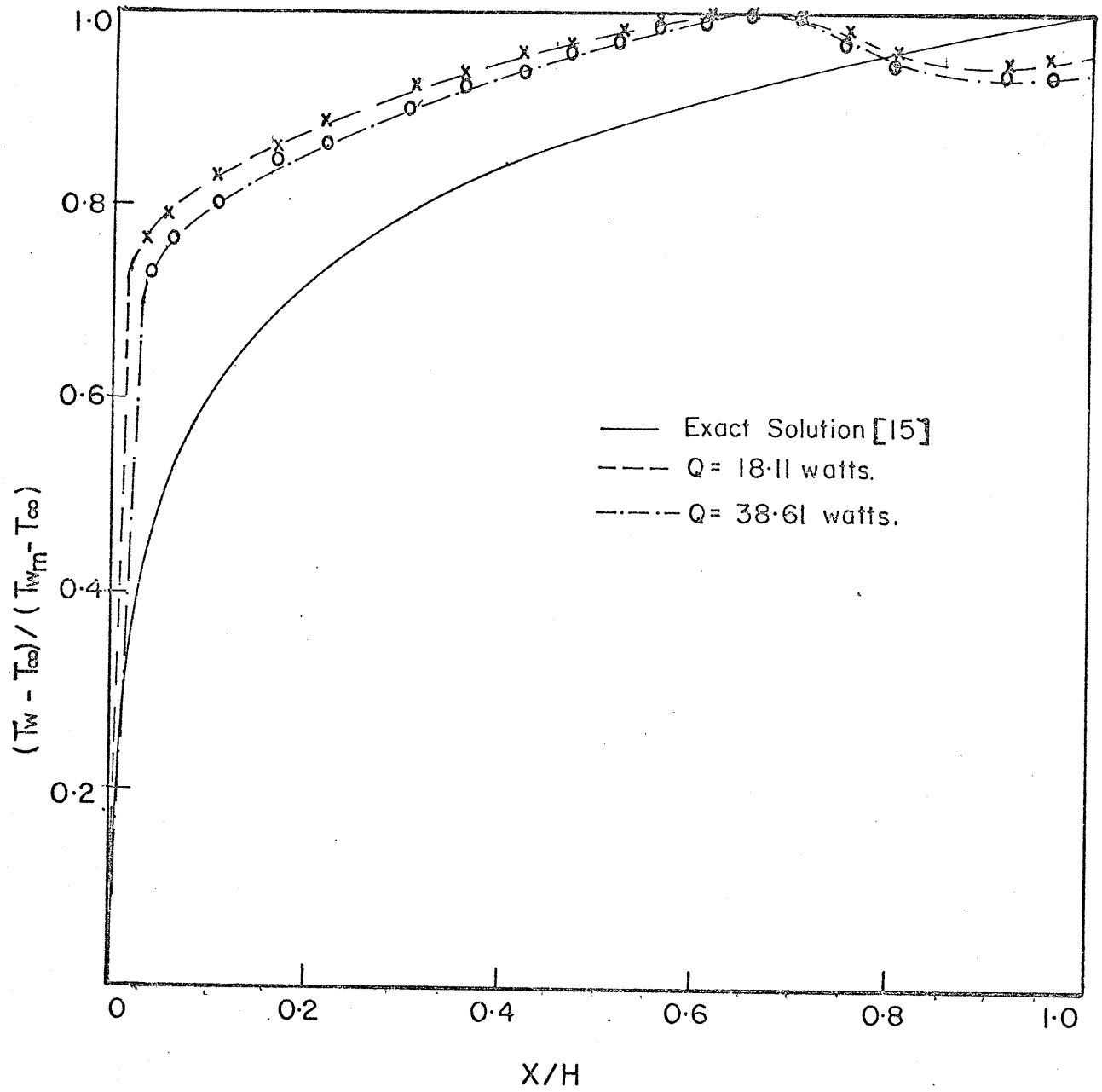

Fig. 7. Non-Dimensional Wall Temperature Distribution.

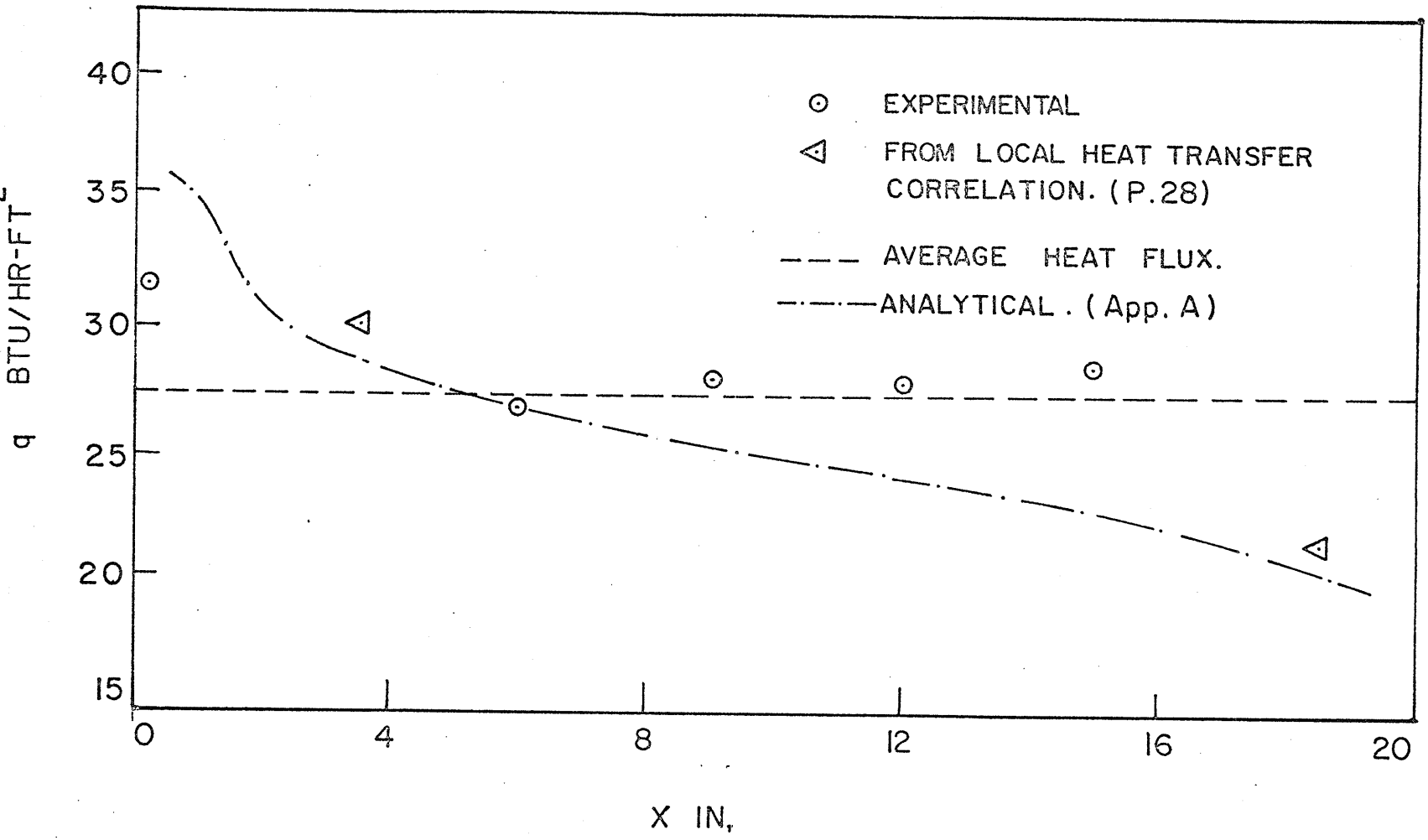

Fig. 8. Local Heat Flux Distribution, Q= 18·11 watts.

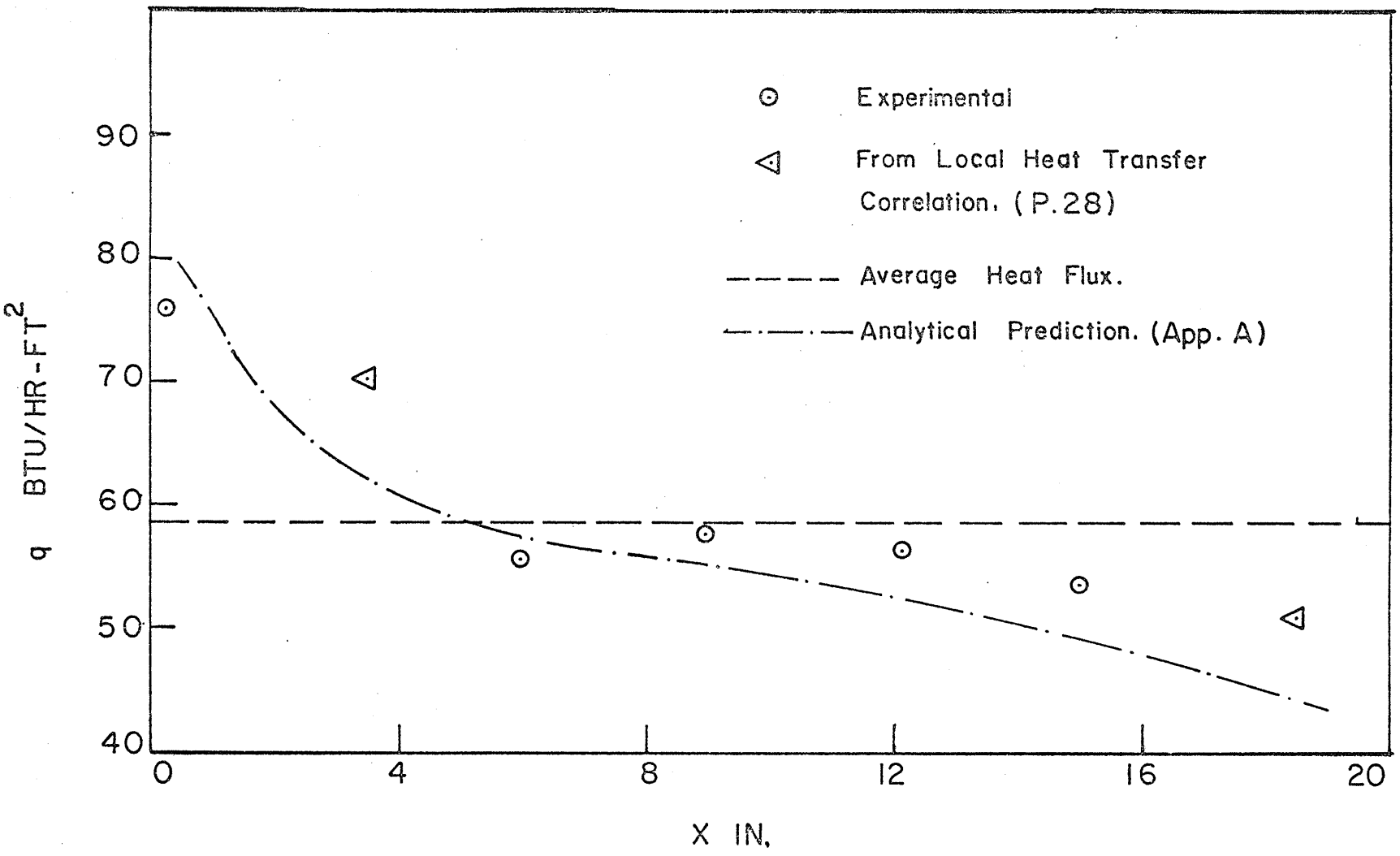

Fig. 9. Local Heat Flux Distribution , Q = 38·61 watts.

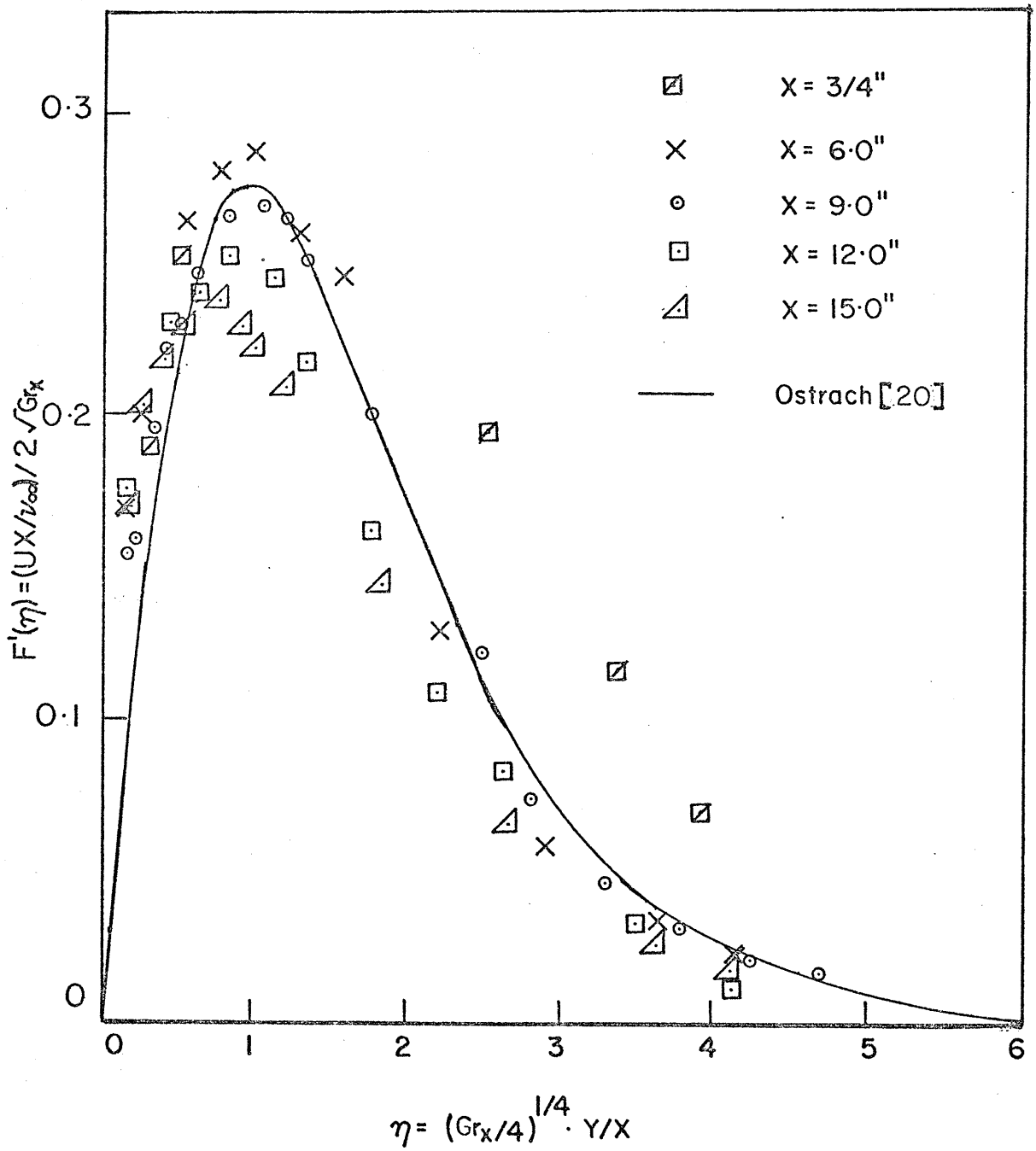

Fig.10. Dimensionless Velocity Distribution for Unbounded Free Convection, Q = 18·11watts.

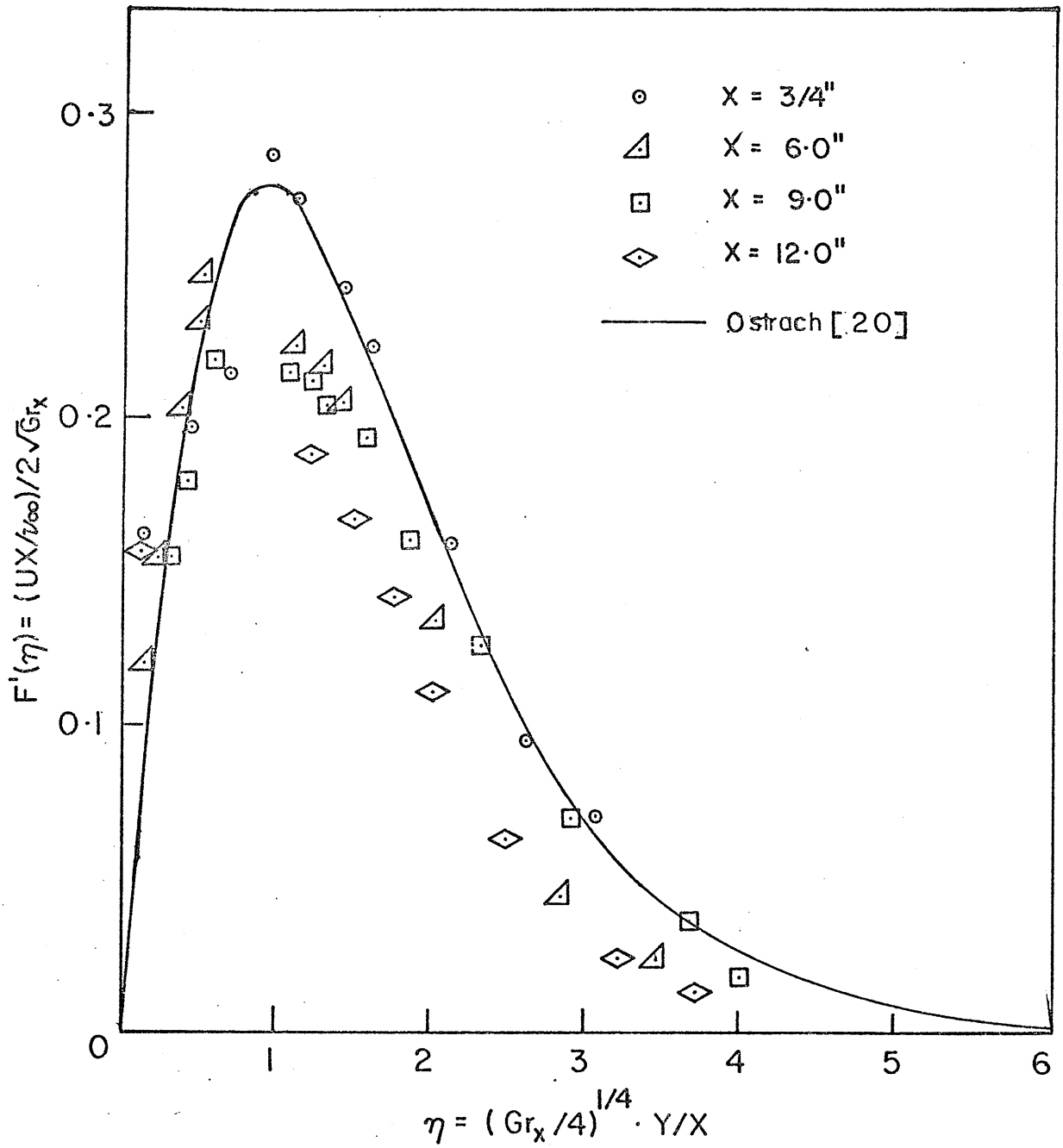

Fig. II. Dimensionless Velocity Distribution for Unbounded Free Convection, Q = 38·61 watts.

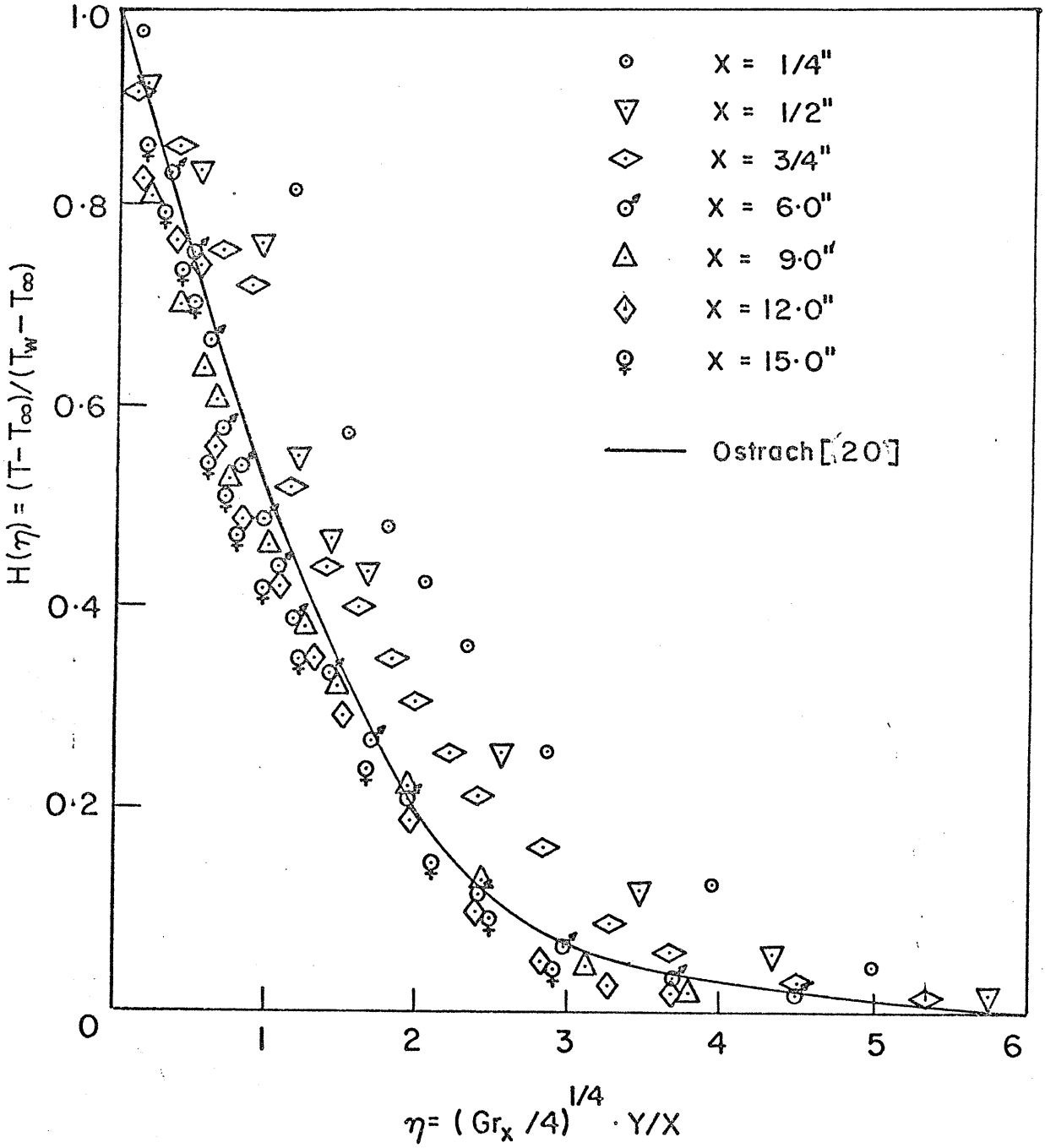

Fig. 12. Dimensionless Temperature Distribution for Unbounded Free Convection , Q = 18·11 watts.

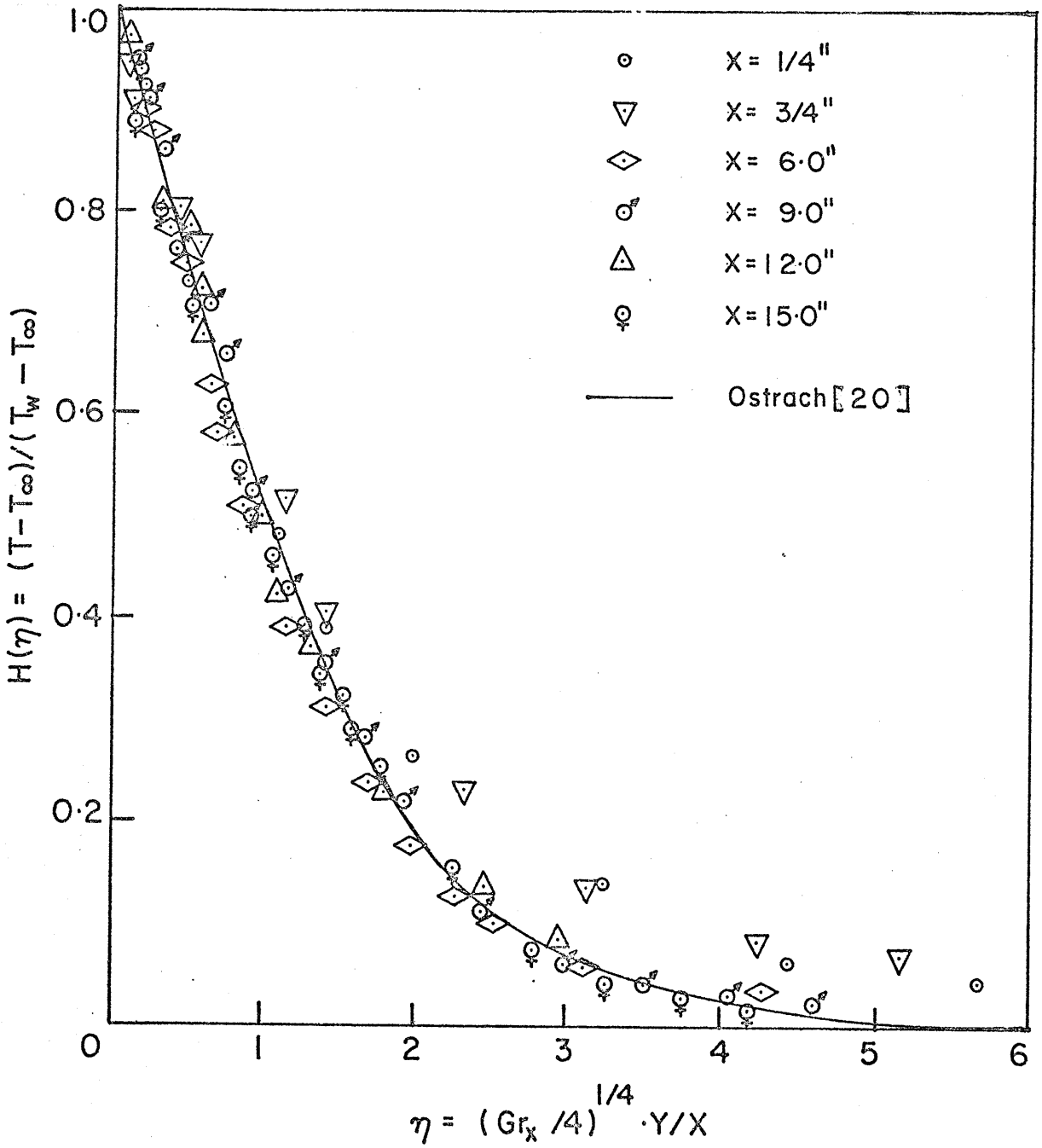

Fig. 13. Dimensionless Temperature Distribution for Unbounded Free Convection , Q = 38·61 watts.

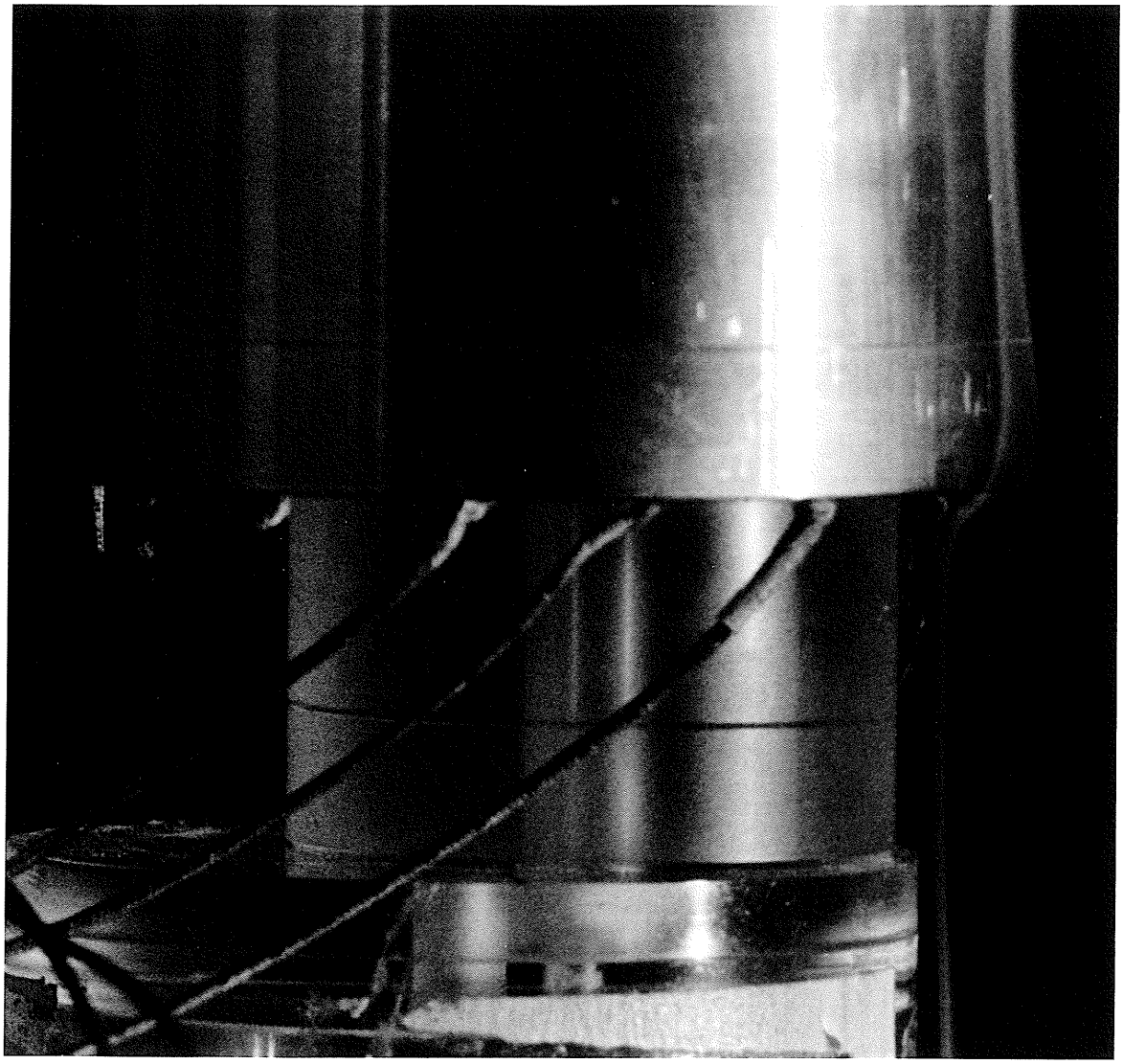

Fig. 14 Photograph Showing Induced Flow Near the Leading Edge.

(Q = 18.11 watts)

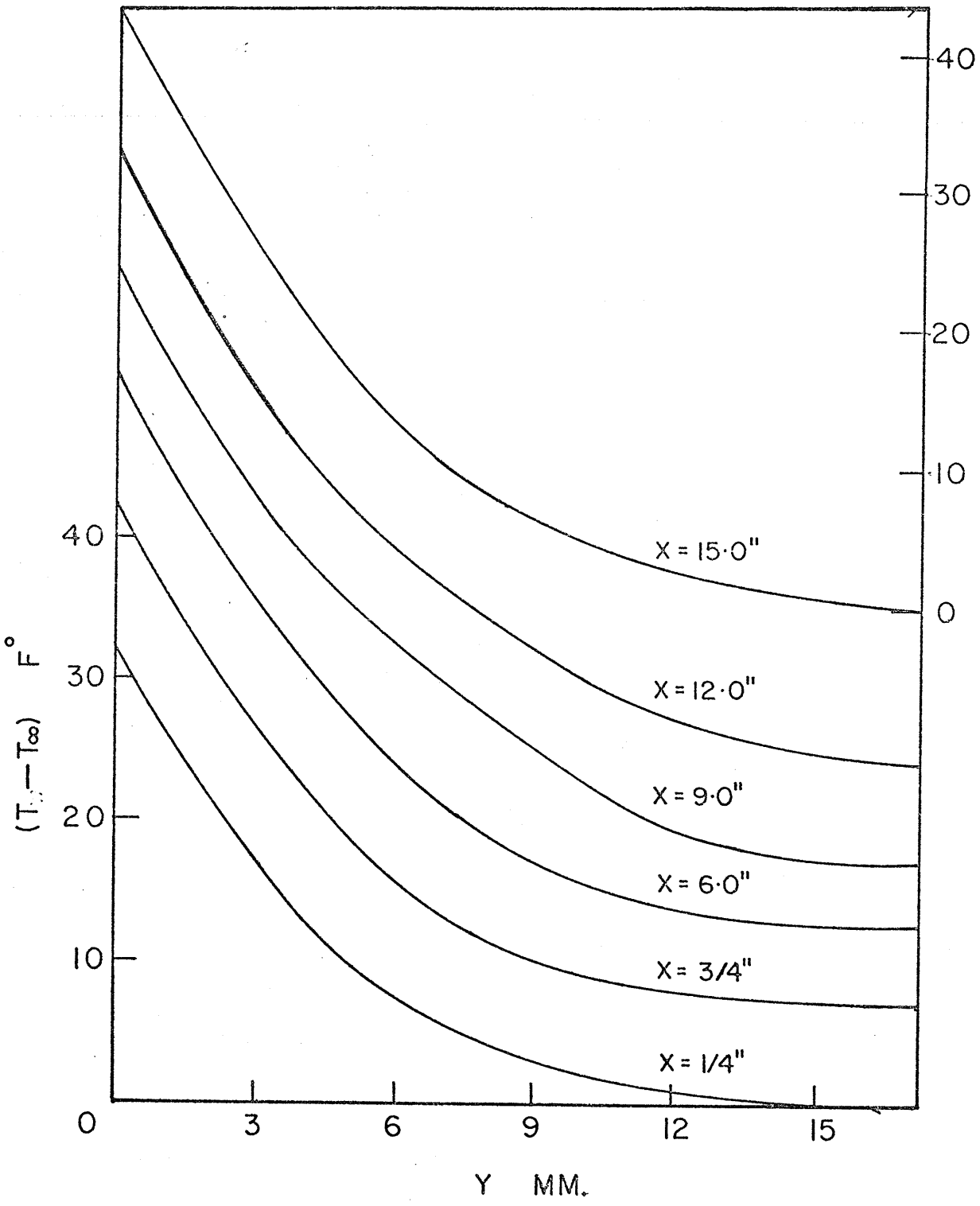

Fig. 15. Boundary Layer Temperature Distribution for Unbounded Free Convection, Q = 18·11 watts.

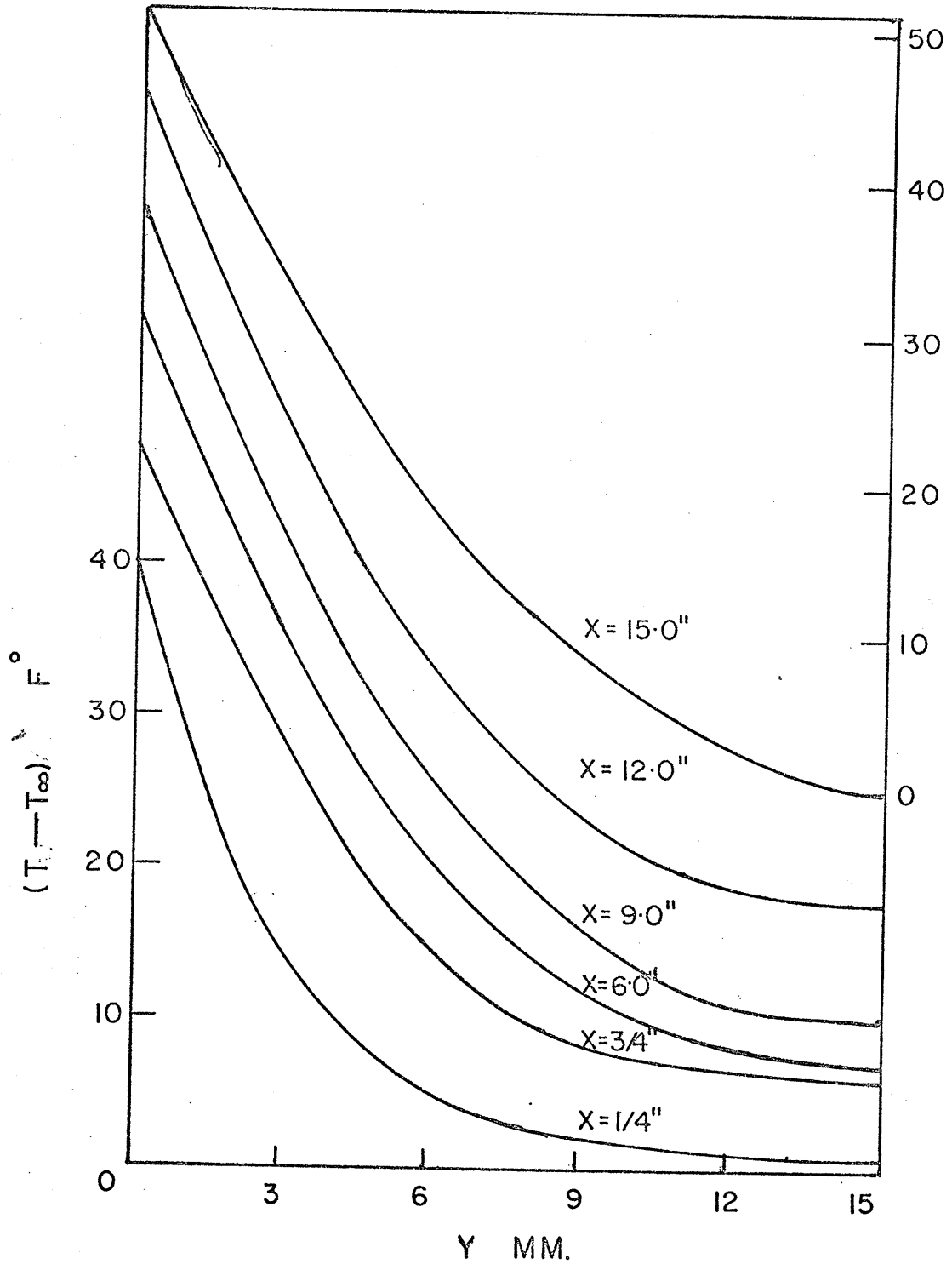

Fig. 16. Boundary Layer Temperature Distribution for Unbounded Free Convection, Q = 38·61 watts.

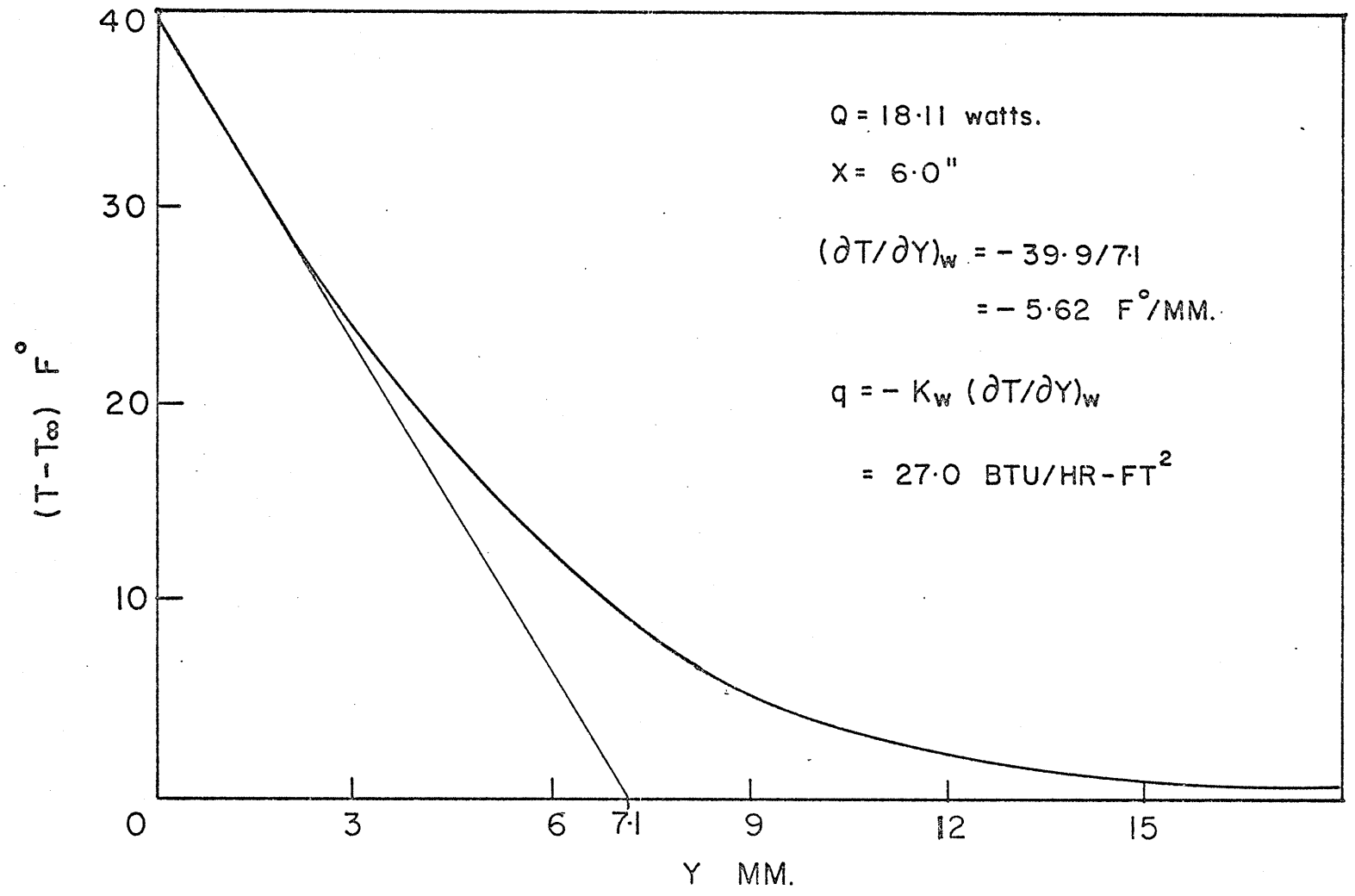

Fig.17. Sample Graph to Determine Local Heat Flux.

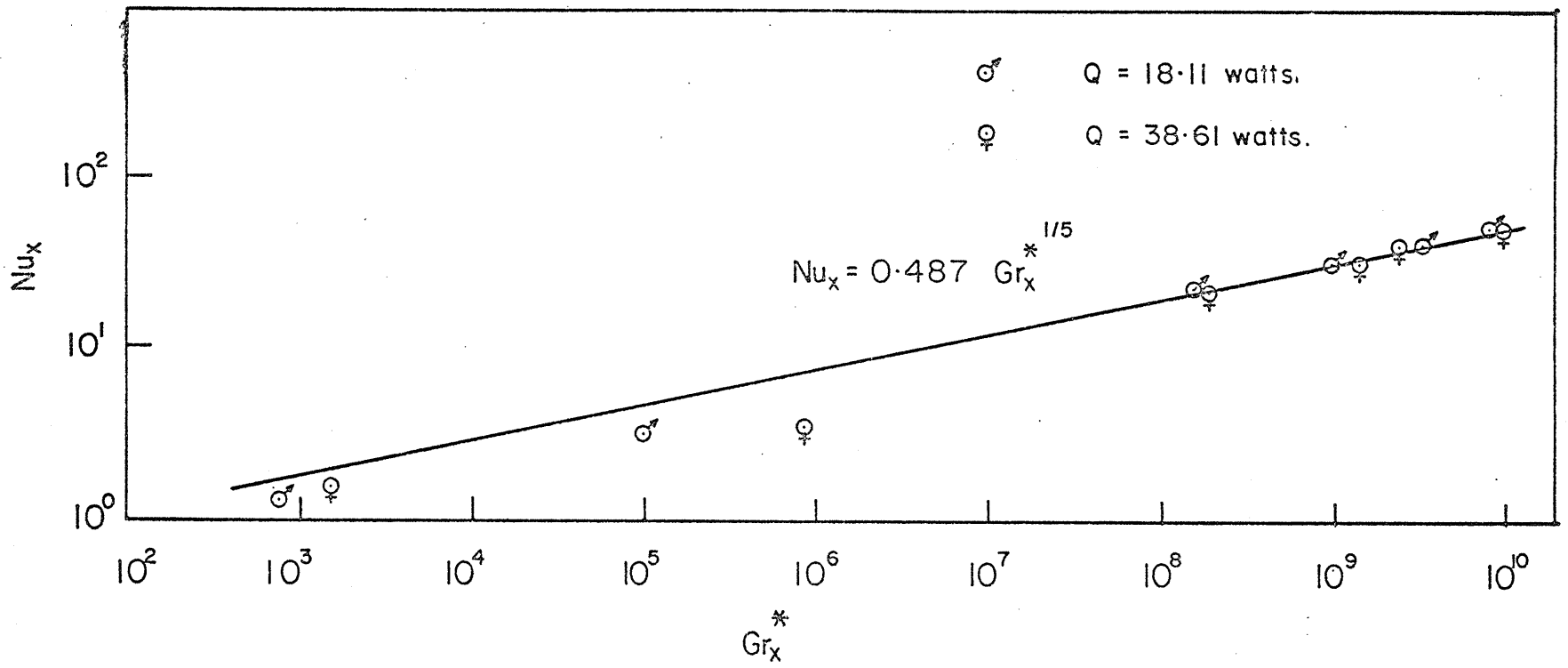

Fig. 18. Local Heat Transfer Results for Unbounded Free Convection.

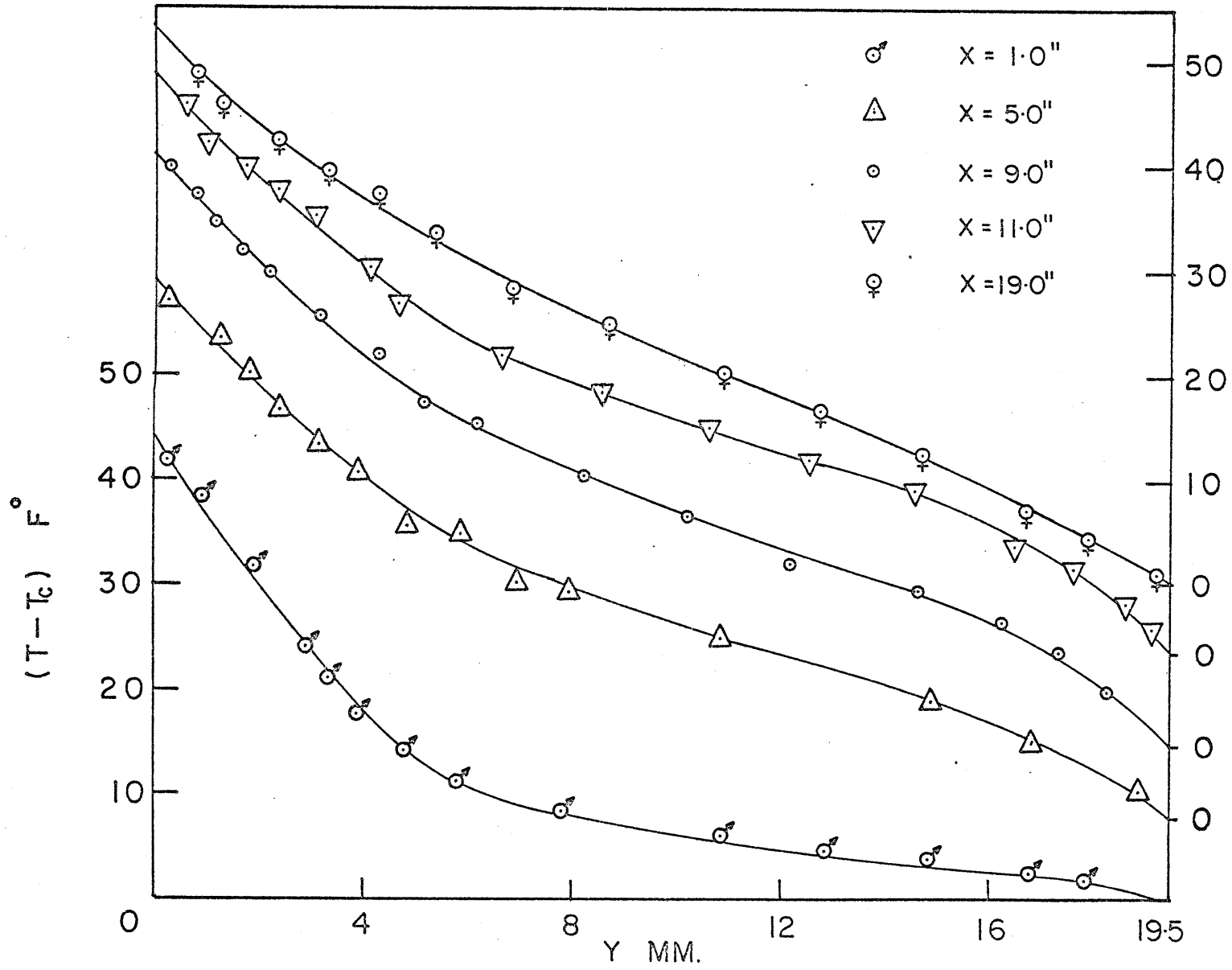

Fig. 19. Temperature Field in Vertical Air Layer, Q = 18·11 watts.

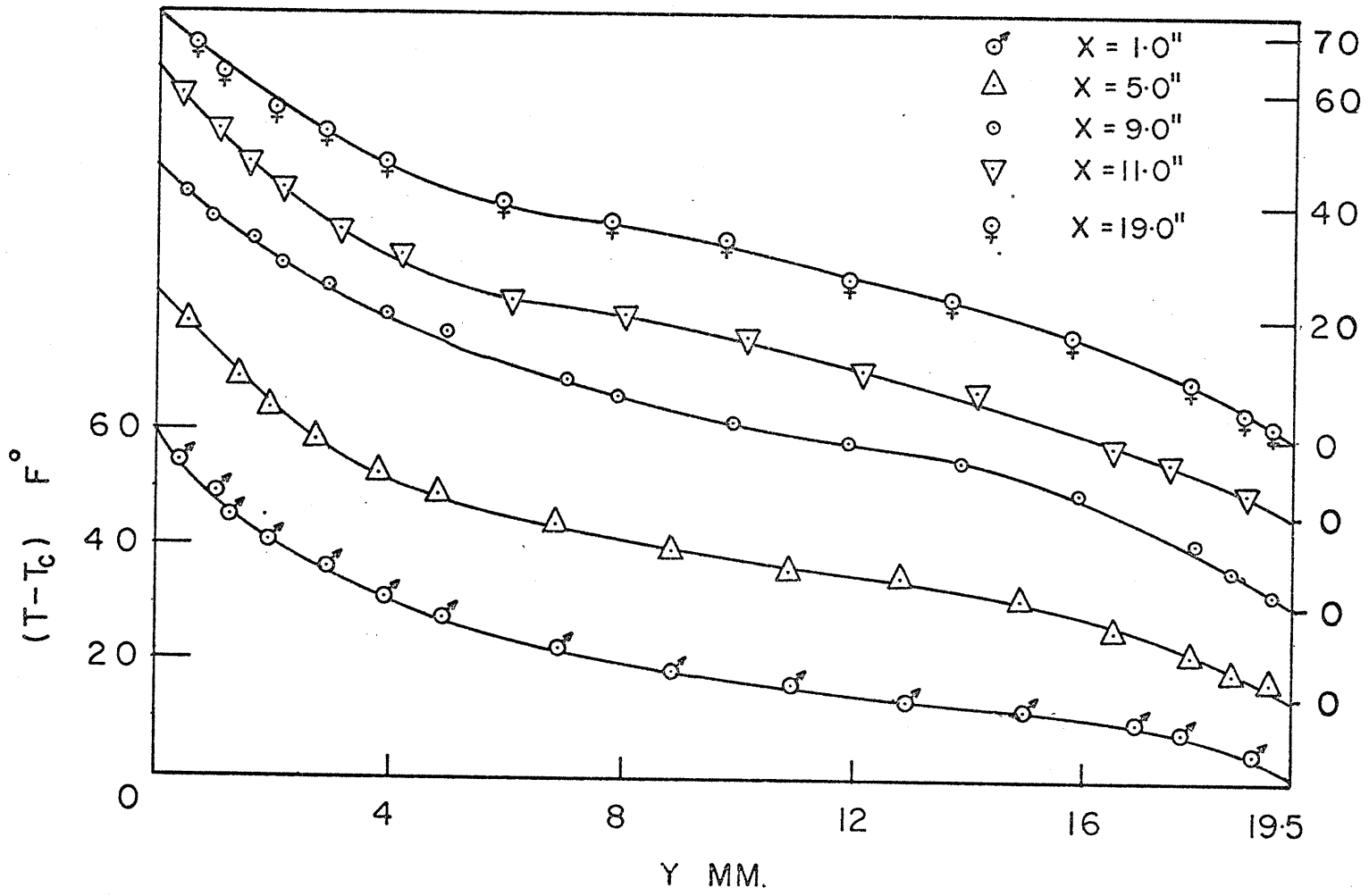

Fig. 20. Temperature Field in Vertical Air Layer, Q = 29·36 watts.

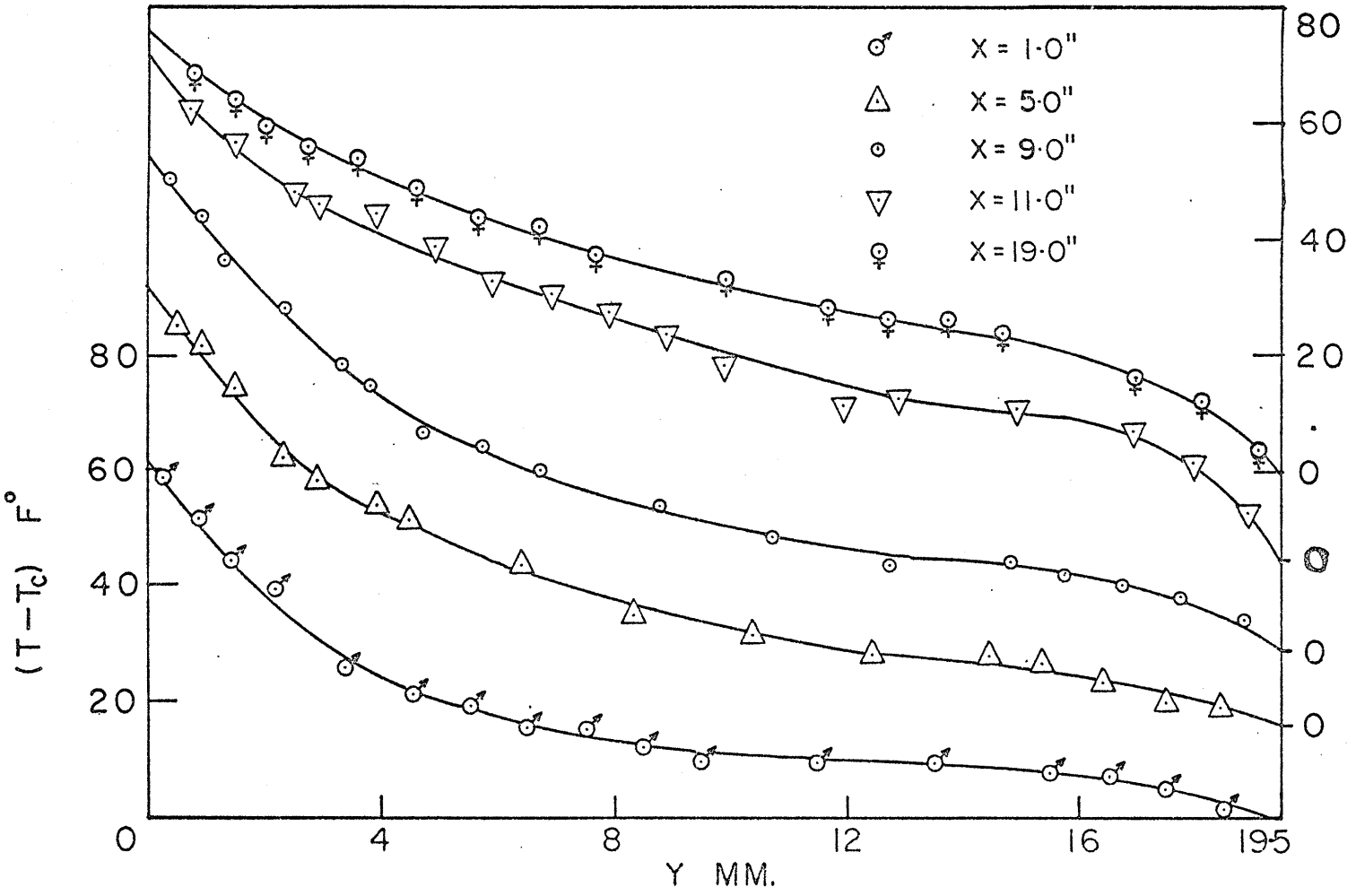

Fig. 21. Temperature Field in Vertical Air Layer, Q = 37·76 watts.

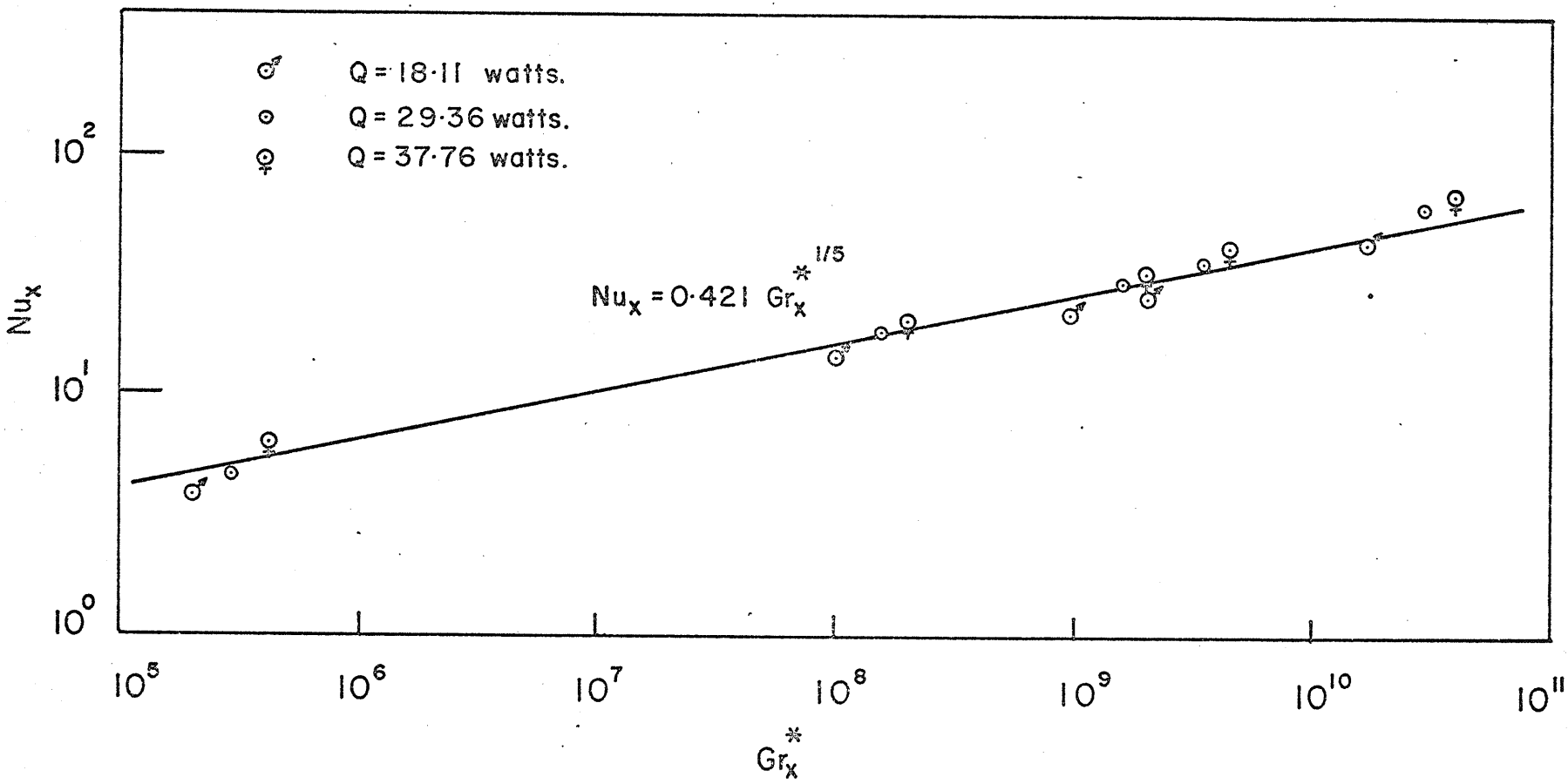

Fig. 22. Local Heat Transfer Results for Vertical Annulus using Modified Grashof Number.

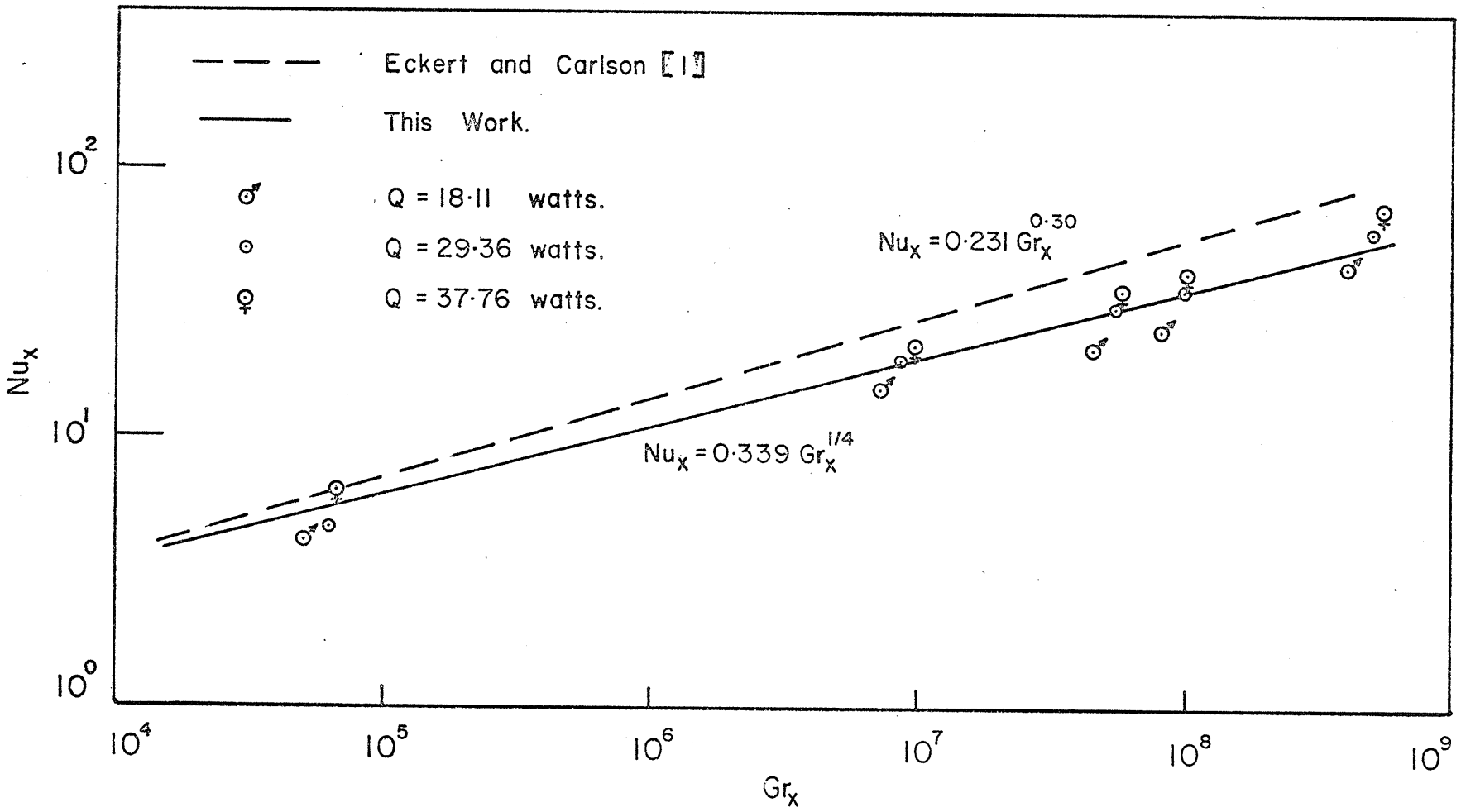

Fig. 23. Local Heat Transfer Results for Vertical Annulus using Conventional Grashof Number.

Symbol	Author	Geometry	Aspect Ratio	Boundary Conditions	Fluid Pr.No.	Range	Remarks
·——·——·	Emery & Chu [10]	Rect.	*26·67	Isothermal	> 3·0	$Gr_w > 10^3$	Expmtl.
··——··——	Eckert & Carlson [1]	–do–	*–do–	–do–	0·72	$Gr_w > 10^5$	–do–
——·——·—	MacGregor & Emery [4]	–do–	*–do–	Mixed	>1·0	$Ra_w > 10^4$	–do–
——·——·——	Sheriff [2]	Annulus R_o/R_i=1.23	*–do–	–do–	< 1·0	$Ra_w > 10^5$	–do–
——	De Vahl Davis & Thomas [6]	–do– R_{out}/R_{in}=2	15·0	Isothermal	0·5 to 5·0	$Ra_w = 10^4$ to 10^5	Numer.
– – – –	–do–	Rect.	–do–	–do–	–do–	–do–	–do–
Present Work:		Annulus R_o/R_i=1·46	26·67	Mixed	0·72	$Gr_w = 2\times10^4$ to 4×10^4	Expmtl.
♀	ϵ =0·29						
⊙	ϵ =0·35						
♂	ϵ =0·40						

* General results plotted for aspect ratio = 26.67

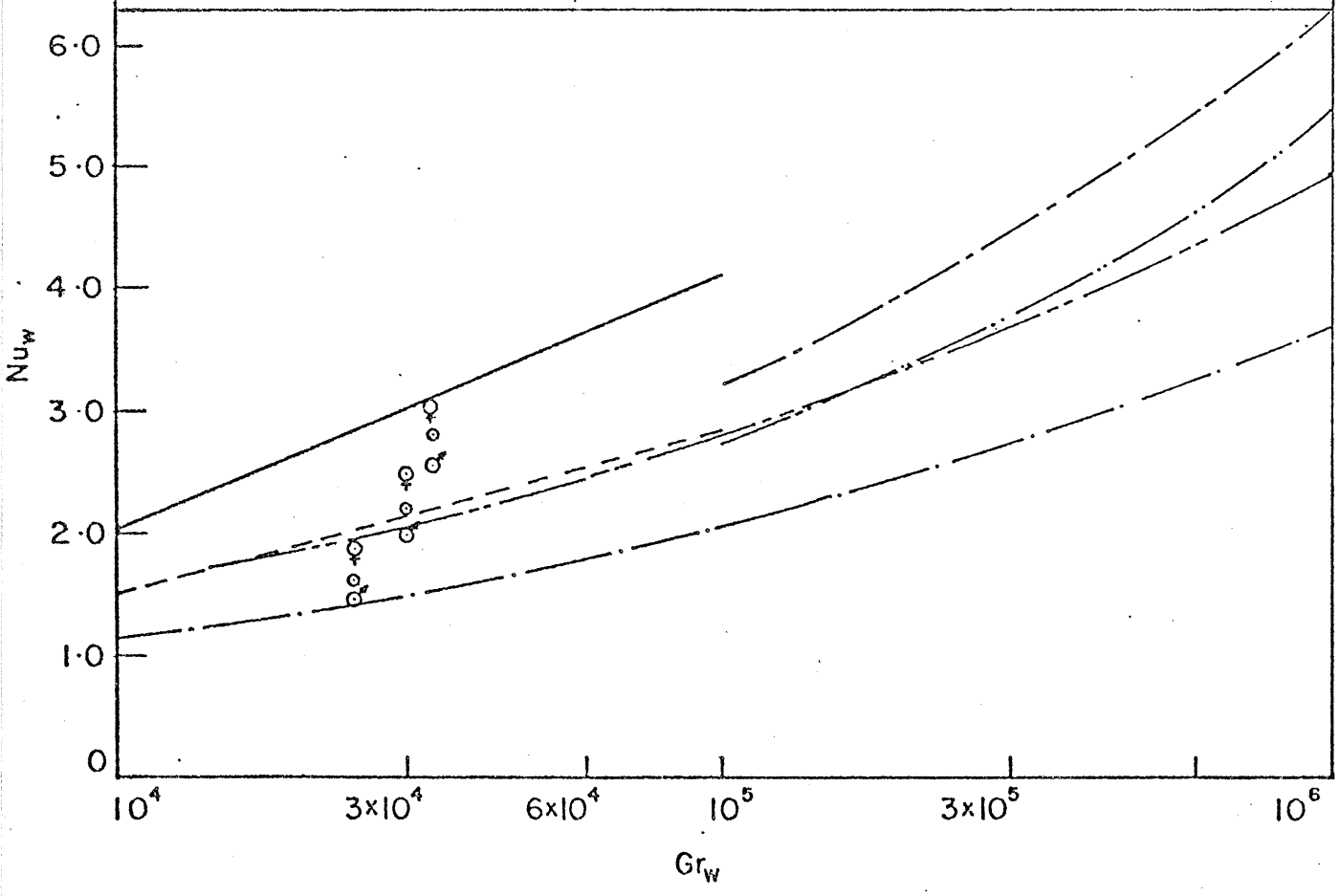

Fig 2.4 Overall Heat Transfer Results for Vertical Annulus.

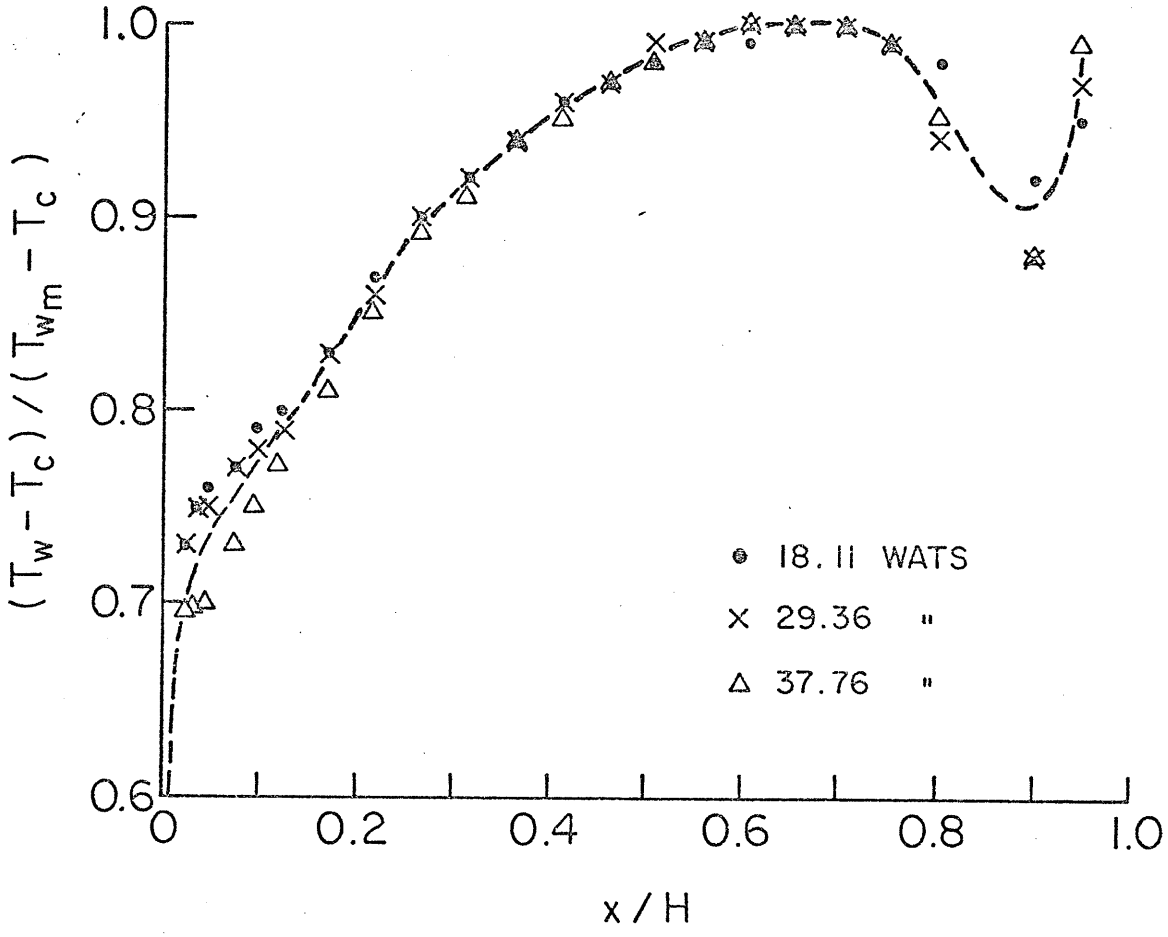

Fig. 25. Non-dimensional Heater Wall Temperature Distribution for Vertical Annulus.

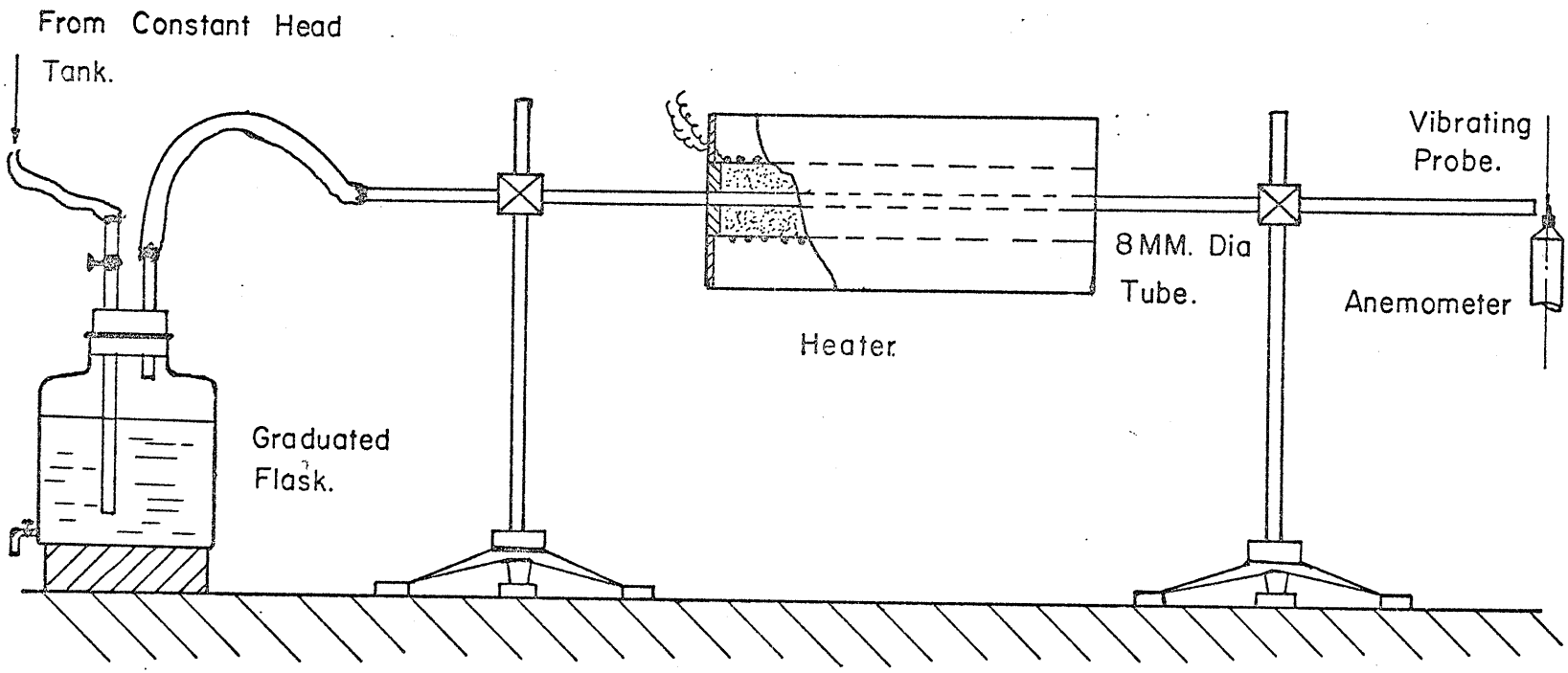

Fig. 26. Sketch of Calibration Equipment for Low Velocity Anemometer.

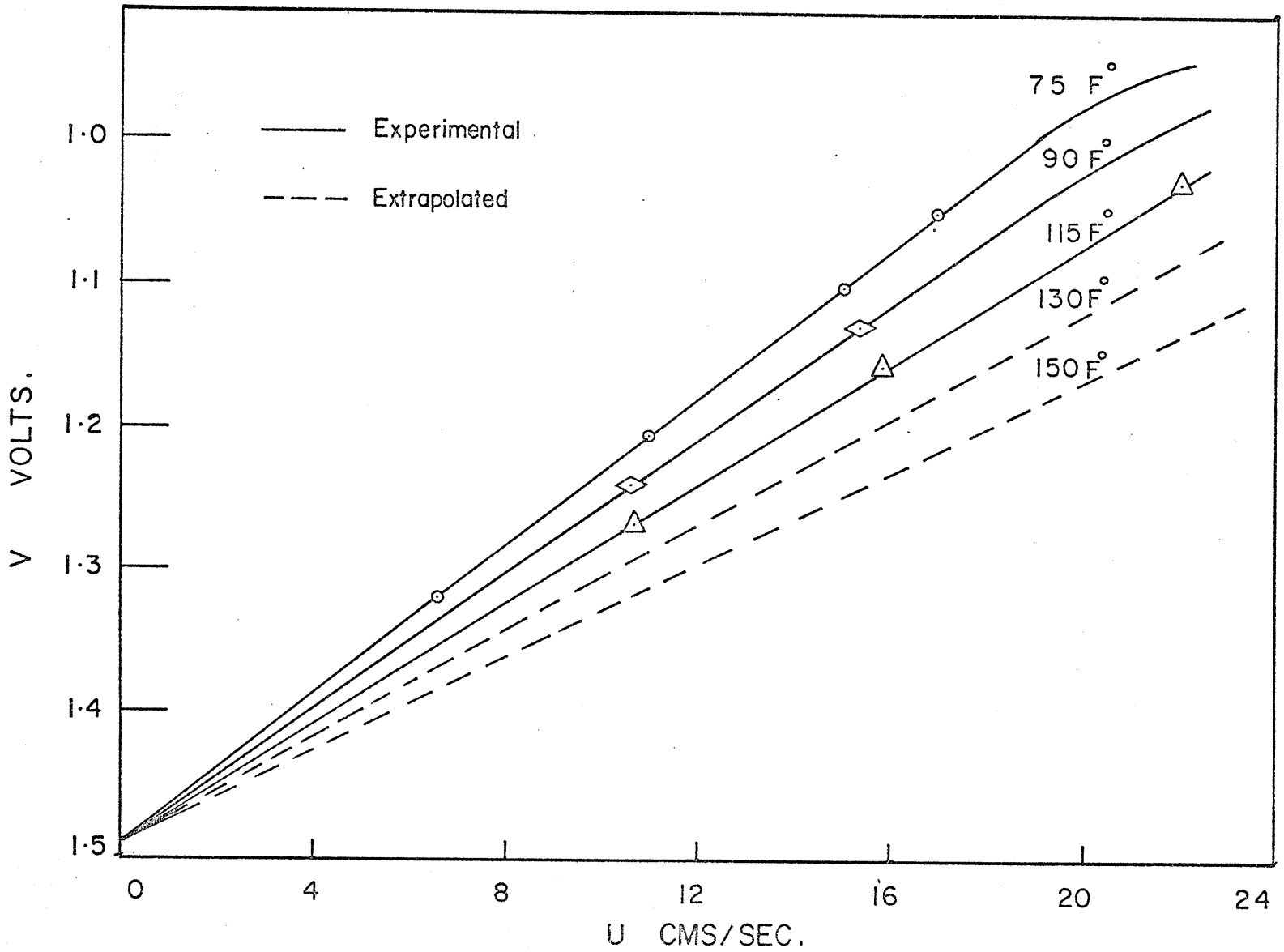

Fig. 27. Calibration Curves for DISA Low Velocity Anemometer.